symmetry

IMPACT FACTOR 2.2

CITESCORE 5.2

Article

Extended Dissipative Approach for Anti-Synchronization of Delayed Inertial Valued Neural Networks via Event-Hybrid Triggered Control with Deception Attacks

Porpattama Hammachukiattikul and Vadivel Rajarathinam

Special Issue

Asymmetric and Symmetric Studies in Nonlinear Dynamics

Edited by

Dr. Rajarathinam Vadivel and Dr. Nallappan Gunasekaran

MDPI

https://doi.org/10.3390/sym18061062

symmetry

MDPI

Article

Extended Dissipative Approach for Anti-Synchronization of Delayed Inertial Valued Neural Networks via Event-Hybrid Triggered Control with Deception Attacks

Porpattama Hammachukiattikul and Vadivel Rajarathinam *

Department of Mathematics, Faculty of Science and Technology, Phuket Rajabhat University, Phuket 83000, Thailand; porpattama@pkru.ac.th
* Correspondence: vadivel.r@pkru.ac.th

Abstract

This paper investigates the problems of anti-synchronization for a class of inertial neural networks (INNs) with time-varying delays under the influence of deception attacks and hybrid triggered control. A novel dynamic hybrid-triggered control (DHTC) scheme is developed to utilize communication resources and enhance network security efficiently for the model INNs. By integrating the extended dissipative approach with Lyapunov–Krasovskii functional (LKF) techniques, new sufficient conditions are established to ensure the quadratic stability of the resulting closed-loop system. The proposed framework not only unifies the anti-synchronization problems but also extends classical passivity, (Q, S, R)-dissipative, H_∞, and $L_2 - L_\infty$ results as special cases. Moreover, the DHTC mechanism dynamically switches between time-triggered and event-triggered modes, reducing unnecessary signal transmissions while maintaining system stability against deception attacks. Finally, simulation results on delayed INNs demonstrate the effectiveness and superiority of the proposed theoretical and control strategy.

Keywords: inertial neural networks; Lyapunov stability; event-triggered; synchronization; extended dissipativity

1. Introduction

Neural networks (NNs) have emerged as powerful computational models inspired by the human brain's structure and function, finding extensive applications in fields such as pattern recognition, optimization, and signal processing [1–3]. These systems are particularly valued for their ability to handle complex, nonlinear dynamics and adapt to varying inputs through learning mechanisms. In recent years, the authors have focused on enhancing the robustness and advancement of NNs, especially in the presence of delays and external disturbances, which are common in real-world implementations like hardware circuits or biological systems [4–8]. For instance, inertial neural networks (INNs) incorporate second-order dynamics to better model physical phenomena, leading to improved performance in tasks requiring memory and inertia effects. The authors in [9] studied synchronization of INNs with time-varying delays via event-based control, while in [10], the authors studied the dissipative theory of delayed memristive INNs. Similarly, in [11], the authors proposed event-triggered strategies for synchronization in the presence of time delays.

Synchronization phenomena in NNs refer to the coordinated behavior where different subsystems align their states over time, while anti-synchronization involves states

Academic Editor: Calogero Vetro

Received: 1 May 2026
Revised: 16 June 2026
Accepted: 17 June 2026
Published: 20 June 2026

evolving in opposite directions, achieving a balanced opposition [12]. In practical terms, synchronization means that the state trajectories of the master and slave systems come together at the same value. Anti-synchronization, on the other hand, is a dynamic behavior in which the magnitudes of the corresponding states are equal but their signs differ. This causes symmetric development with regard to the origin. These concepts are crucial in secure communications, where synchronization enables data encoding and decoding, and anti-synchronization provides additional layers of encryption by mirroring signals inversely. Recent advancements have explored these in delayed neural networks, highlighting how time-varying delays can influence stability and convergence rates. In [13], anti-synchronization control has been studied for a class of memristive recurrent neural networks, whereas reference [14] examined synchronization and anti-synchronization of a fractional chaotic financial system. The researchers in [15] further explored synchronization of Markov jump INNS with the non-reduced-order method.

The extended dissipative framework offers a unified approach to analyze system performance under various criteria, including H_∞ control, passivity, and dissipativity, by encompassing them within a single inequality involving adjustable matrices [16]. This method is especially useful for handling disturbances and ensuring robustness in neural network designs. Adjusting parameters like Φ_1 to Φ_4 allows for flexible evaluation of energy dissipation and storage, making it suitable for systems with delays and nonlinear activations. In [17], the authors proposed the event-triggered extended dissipative control for networked singular systems, while in [18], the framework was extended to an extended dissipative fractional-order chaotic NNs. The work reference [19] focused on the related event-triggered dissipativity filtering for NNs.

Traditional network configurations often lean on time-triggered control approaches, where the sensing of the system state and the control updates happen strictly at those preset, fairly uniform time intervals [20]. In a sense, this periodic transmission scheme gives high predictability; it also makes stability reasoning easier in a deterministic way, and it keeps the system monitoring in the expected conditions. Yet, the moment data packets keep flowing regardless of whether the system state has significantly changed, the whole time-triggered method starts looking pretty wasteful; it can overload the communication links with redundant bits, over and over [21–23]. So to reduce this bandwidth squeeze, event-triggered control strategies have revolutionized resource management in networked systems by transmitting data only when necessary, thus reducing communication overhead while maintaining performance [12,24–26]. When combined with deception attacks—malicious alterations to transmitted signals—these strategies must incorporate security measures to detect and mitigate cyber threats [27,28]. Hybrid-triggered mechanisms, blending time- and event-based triggers, offer adaptability, often modeled with Bernoulli distributions for random switching. The study in [29] designed event-triggered synchronization for NNs under deception attacks, while in [30], the researchers proposed a nonlinear networked control system with the same deception attacks. Utilizing the same attacks, authors in [31] concentrated on event-triggered mechanisms of Photovoltaic Microgrids.

Motivated by these observations, this paper proposes a comprehensive framework for the analysis and control of delayed INNs under deception attacks using an extended dissipative approach. Specifically, we design a dynamic hybrid-triggered control (DHTC) strategy whereby the controller can adaptively switch between time-triggered and event-triggered transmissions according to both the state information and network conditions. The dissipativity-based analysis offers a unified framework, encompassing classic stability criteria such as passivity, (Q, S, R)-dissipative, H_∞, and $L_2 - L_\infty$ as special cases. To cope with time-varying delays and deception attacks simultaneously, we construct a refined

Lyapunov–Krasovskii functional and derive delay-dependent stability criteria in terms of linear matrix inequalities (LMIs).

The following is a summary of this work's main contributions:

1. We propose a novel dynamic hybrid-triggered control strategy to achieve both anti-synchronization for delayed INNs subject to deception attacks. Figure 1 represents the schematic diagram of the proposed model.
2. We develop an extended dissipative analysis framework, which unifies passivity, $L_2 - L_\infty$, H_∞, and (Q, S, R)-dissipativity conditions as special cases.
3. We derive new delay-dependent stability criteria via the Lyapunov–Krasovskii functional (LKF) technique and the reciprocally convex approach, which provide less conservative results.
4. We present a simulation example to verify the effectiveness, reduced communication load, and robustness of the proposed control mechanism.

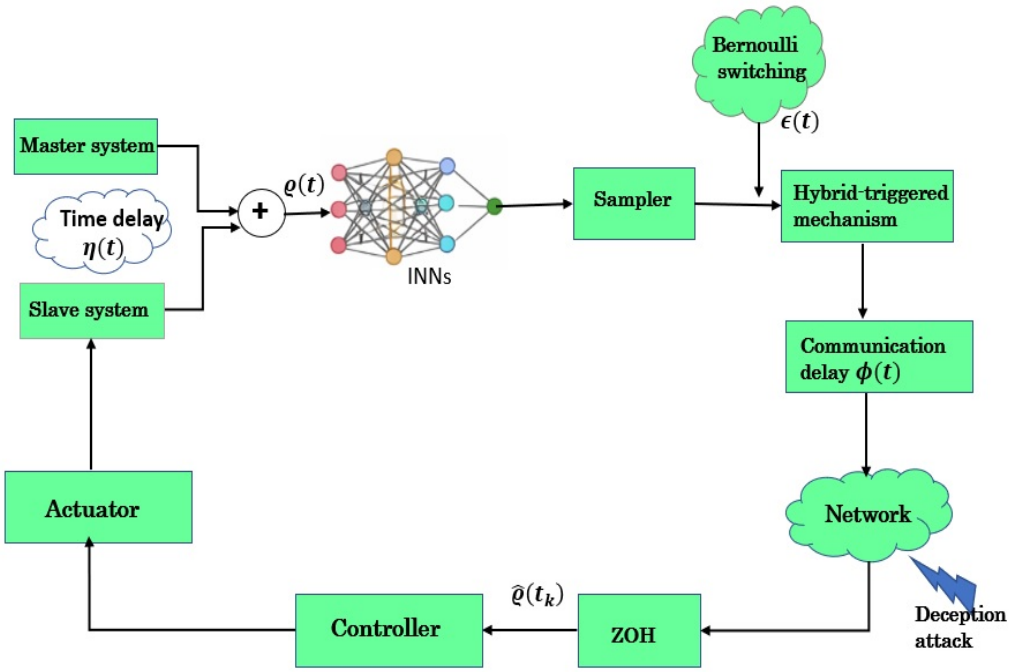

Figure 1. Block diagram of the proposed hybrid-triggered control scheme with deception attacks.

2. Problem Formulation

This article will examine the INNs model, which is defined as follows:

$$\begin{cases} \ddot{\hat{x}}_1(t) = -\aleph\dot{\hat{x}}_1(t) - \mathcal{A}\hat{x}_1(t) + \mathcal{B}g(\hat{x}_1(t)) + \mathcal{C}g(\hat{x}_1(t-\eta(t))), \\ y_1(t) = \hat{x}_1(t), \end{cases} \tag{1}$$

where the state variable is denoted by $\hat{x}_1(t) \in \mathbb{R}^n$; the second derivative term of the system (1) is denoted by inertia term; the output is represented by $y_1(t)$; the diagonal matrices are $\mathcal{A} > 0$ and $\aleph > 0$; $\mathcal{B}$ and $\mathcal{C}$ are the connection weight matrices; $g(\hat{x}_1(t)), g(\hat{x}_1(t-\eta(t))) \in \mathbb{R}^n$ are indicated as activation functions; $\eta(t)$ denotes the time-varying delays with $0 \leq \eta(t) \leq \eta, \dot{\eta}(t) \leq \widetilde{\mu} < 1$, where $\eta > 0$ and $\widetilde{\mu} > 0$ are constants. $\hat{x}_1(t) = \phi(s), \frac{d\hat{x}_1(s)}{dt} = \tau(s)$ indicate the initial conditions of (1), where $s \in [-\eta, 0]$ and $\phi(s), \tau(s)$ are continuous.

Assumption 1. *The following Lipschitz condition is satisfied by the neuron activation function g_j, scalar $\ell_j > 0$, such that for $j = 1, 2, 3, \cdots, n$, $\|g_j(\hat{x}_1) - g_j(\bar{x}_1)\| \leq \ell_j \|\hat{x}_1 - \bar{x}_1\| \forall \hat{x}_1, \bar{x}_1 \in \mathbb{R}$.*

Define $h(t) = \frac{d\hat{x}_1(t)}{dt} + \hat{x}_1(t)$, then (1) can be outlined as master system

$$\begin{cases} \frac{d\hat{x}_1(t)}{dt} & = -\hat{x}_1(t) + h(t), y_1(t) = \hat{x}_1(t), \\ \frac{dh(t)}{dt} & = -\Omega\hat{x}_1(t) - \Theta h(t) + \mathcal{B}g(\hat{x}_1(t)) + \mathcal{C}g(\hat{x}_1(t - \eta(t))), \end{cases} \tag{2}$$

where $\Omega = \mathcal{A} - \aleph + I, \Theta = \aleph - I$. The equivalent slave system may be written as

$$\begin{cases} \frac{d\hat{x}_2(t)}{dt} & = -\hat{x}_2(t) + \hat{h}(t) + \mathcal{U}_1(t), y_2(t) = \hat{x}_2(t) \\ \frac{d\hat{h}(t)}{dt} & = -\Omega\hat{x}_2(t) - \Theta\hat{h}(t) + \mathcal{B}g(\hat{x}_2(t)) + \mathcal{C}g(\hat{x}_2(t - \eta(t))) + \mathcal{U}_2(t) + H_1 w(t), \end{cases} \tag{3}$$

where $\mathcal{U}_1(t)$ and $\mathcal{U}_2(t)$ are the controllers to be designed. Let $\hat{x}_1(t) = \text{col}\{\hat{x}_{11}(t), \hat{x}_{12}(t), \cdots, \hat{x}_{1n}(t)\}$ and $g(\hat{x}_1(t)) = \text{col}\{g_1(\hat{x}_{11}(t)), g_2(\hat{x}_{12}(t)), \cdots, g_n(\hat{x}_{1n}(t))\}$. Let $\varpi(t) = \hat{x}_2(t) + \hat{x}_1(t), \wp(t) = \hat{h}(t) + h(t), y(t) = y_2(t) + y_1(t)$, the anti-synchronization error system from (2) and (3) is given as follows

$$\begin{cases} \frac{d\varpi(t)}{dt} & = -\varpi(t) + \wp(t) + \mathcal{U}_1(t), \\ y(t) & = \varpi(t) \\ \frac{d\wp(t)}{dt} & = -\Omega\varpi(t) - \Theta\wp(t) + \mathcal{B}\mathcal{F}(\varpi(t)) + \mathcal{C}\mathcal{F}(\varpi(t - \eta(t))) + \mathcal{U}_2(t) + H_1 w(t), \end{cases} \tag{4}$$

where $\mathcal{F}(\varpi(t)) = g(\hat{x}_2(t)) + g(\hat{x}_1(t))$ and $\mathcal{F}(\varpi(t - \eta(t))) = g(\hat{x}_2(t - \eta(t))) + g(\hat{x}_1(t - \eta(t)))$. Then, (4) can be written as

$$\begin{cases} \frac{dx(t)}{dt} & = -\hat{\mathcal{A}}x(t) + \hat{\mathcal{B}}\hat{\mathcal{F}}(x(t)) + \hat{\mathcal{C}}\hat{\mathcal{F}}(x(t - \eta(t))) + \mathcal{U}(t) + \hat{H}_1 w(t), \\ y(t) & = \hat{\mathcal{D}}x(t), \end{cases} \tag{5}$$

where $x(t) = \begin{bmatrix} \varpi(t) \\ \wp(t) \end{bmatrix}, \hat{\mathcal{F}}(x(t)) = \begin{bmatrix} \mathcal{F}(\varpi(t)) \\ 0 \end{bmatrix}, \hat{\mathcal{F}}(x(t - \eta(t))) = \begin{bmatrix} \mathcal{F}(\varpi(t - \eta(t))) \\ 0 \end{bmatrix}, \hat{\mathcal{A}} = \begin{bmatrix} I & -I \\ \Omega & \Theta \end{bmatrix}, \hat{\mathcal{C}} = \begin{bmatrix} 0 & 0 \\ \mathcal{C} & 0 \end{bmatrix}, \hat{\mathcal{B}} = \begin{bmatrix} 0 & 0 \\ \mathcal{B} & 0 \end{bmatrix}, \mathcal{U}(t) = \begin{bmatrix} \mathcal{U}_1(t) \\ \mathcal{U}_2(t) \end{bmatrix}, \hat{H}_1 = \begin{bmatrix} 0_{n\times n} \\ H_1 \end{bmatrix} \in \mathbb{R}^{2n\times n}, w(t) = w(t) \in \mathbb{R}^n, \hat{\mathcal{D}} = \begin{bmatrix} I_n & 0_{n\times n} \end{bmatrix} \in \mathbb{R}^{n\times 2n}$.

3. Dynamic Hybrid-Triggered Strategy with Deception Attacks

This part talks about a dynamic hybrid-triggered transmission strategy that incorporates an adaptive event-triggered (ET) scheme with a periodic time-triggered scheme. The goal is to lower the communication load and improve control performance. The hybrid-triggered device and the zero-order hold (ZOH) are put between the sampler and the controller, as shown in Figure 1. The two ways of communicating are chosen by a signal that follows a Bernoulli distribution.

3.1. Hybrid Dynamic Event-Triggered Transmission

When the time-triggered mechanism is engaged, the sampled state sent to the controller, incorporating a communication delay, may be expressed as

$$x_1(t) = x(t_n\tilde{q}), \quad t \in [t_n\tilde{q} + \kappa_n, t_{(n+1)}\tilde{q} + \kappa_{n+1}), n \in \mathbb{Z}, \tag{6}$$

where $\tilde{q} > 0$ is the sampling period, $t_n\tilde{q}$ denotes the latest sampling instant, and κ_n, κ_{n+1} are communication delays. Define the piecewise function

$$\phi(t) = t - t_n\tilde{q}, \quad t \in [t_n\tilde{q} + \kappa_n,\ t_{(n+1)}\tilde{q} + \kappa_{n+1}),$$

with $0 < \phi(t) < \phi_M + \tilde{q} = \phi_2$. Then, (6) can be reformulated as

$$x_1(t) = x(t - \phi(t)), \quad t \in [t_n\tilde{q} + \kappa_n,\ t_{(n+1)}\tilde{q} + \kappa_{n+1}),\ n \in \mathbb{Z}. \tag{7}$$

When the adaptive ET mechanism is selected, the transmitted state is

$$x_2(t) = x(t_m\tilde{q}), \quad t \in [t_m\tilde{q} + \kappa_m,\ t_{m+1}\tilde{q} + \kappa_{m+1}),\ m \in \mathbb{Z}, \tag{8}$$

where $t_m\tilde{q}$ denotes the latest triggered instant. Describe the error between the current sampled signal and the latest released signal as

$$e(t) = x(t_m\tilde{q} + l\tilde{q}) - x(t_m\tilde{q}). \tag{9}$$

The sampled signal present instant $x(t_m\tilde{q} + l\tilde{q})$ may be released or not dependent on the subsequent inequality

$$e^T(t)He(t) \geq v(t)\, x^T(t_m\tilde{q})Hx(t_m\tilde{q}), \tag{10}$$

where $H > 0$ and the threshold $v(t)$ evolves according to

$$\dot{v}(t) = \left(\frac{1}{v^2(t)} - \frac{v_0}{v(t)}\right)e^T(t)He(t), \tag{11}$$

with $v_0 > 0$ a constant, and $v(t) \in [0, v_2]$ for some positive bounds v_2.

For convenience, the interval $[t_m + \kappa_m,\ t_{m+1} + \kappa_{m+1})$ is divided into subintervals

$$\begin{aligned}
\Delta_1 &= [t_m\tilde{q} + \kappa_m,\ t_m\tilde{q} + \tilde{q} + \kappa_m),\\
\Delta_2 &= [t_m\tilde{q} + \tilde{q} + \kappa_m,\ t_m\tilde{q} + 2\tilde{q} + \kappa_m),\\
&\vdots\\
\Delta_{\bar{\zeta}} &= [t_m\tilde{q} + (\bar{\zeta} - 1)\tilde{q} + \kappa_m,\ t_{m+1}\tilde{q} + \kappa_{m+1}),
\end{aligned} \tag{12}$$

where $\bar{\zeta} = \min\{\zeta \mid t_m\tilde{q} + \zeta\tilde{q} + \kappa_m \geq t_{m+1}\tilde{q} + \kappa_{m+1}\}$. The transmitted state can be equivalently written as

$$x_2(t) = x(t - \phi(t)) - e(t), \quad t \in [t_m\tilde{p} + \kappa_m,\ t_{m+1}\tilde{p} + \kappa_{m+1}),\ m \in \mathbb{Z}. \tag{13}$$

Under the dynamic switching scheme, the signal received by the controller is

$$\hat{x}(t) = \varepsilon(t)x(t - \phi(t)) + (1 - \varepsilon(t))[x(t - \phi(t)) - e(t)], \tag{14}$$

where $\varepsilon(t)$ is a Bernoulli random variable with distribution

$$\begin{aligned}
\Pr\{\varepsilon(t) = 1\} &= \mathbb{E}\{\varepsilon(t)\} = \hat{\varepsilon},\\
\Pr\{\varepsilon(t) = 0\} &= 1 - \hat{\varepsilon},
\end{aligned} \tag{15}$$

with variance $\mathbb{E}\{(\varepsilon(t) - \hat{\varepsilon})^2\} = \hat{\varepsilon}(1 - \hat{\varepsilon}) = a^2$.

3.2. Deception Attacks

Deception attacks can affect both the sensor-to-controller and controller-to-actuator channels. From the system perspective, such attacks cause abnormal actuator signals, and the exact attack location cannot be distinguished. Thus, it is reasonable to consider both as actuator deception attacks. The attacked signal is modeled as

$$\mathcal{U}(t) = (1-\delta(t))K\hat{x}(t) + \delta(t)K\,g(x(t-\phi(t))), \tag{16}$$

where K is a feedback gain, $g(\cdot)$ is a nonlinear function satisfying

$$g^T(x(t-\phi(t)))g(x(t-\phi(t))) \leq x^T(t)G^TGx(t), \tag{17}$$

for some constant matrix G. The random variable $\delta(t) \in \{0,1\}$ follows

$$\Pr\{\delta(t)=1\} = \hat{\delta},\ \Pr\{\delta(t)=0\} = 1-\hat{\delta}, \tag{18}$$

with variance $\mathbb{E}\{(\delta(t)-\hat{\delta})^2\} = \hat{\delta}(1-\hat{\delta}) = b^2$.

Therefore, combining (5) and (16)–(18), we get

$$\begin{aligned}
\frac{dx(t)}{dt} &= -\hat{\mathcal{A}}x(t) + \hat{\mathcal{B}}\hat{\mathcal{F}}(x(t)) + \hat{\mathcal{C}}\hat{\mathcal{F}}(x(t-\eta(t))) \\
&\quad + (1-\delta(t))K\hat{x}(t) + \delta(t)K\,g(x(t-\phi(t))) + \hat{H}_1 w(t), \\
\hat{x}(t) &= \varepsilon(t)x(t-\phi(t)) + (1-\varepsilon(t))[x(t-\phi(t)) - e(t)], \\
y(t) &= \hat{\mathcal{D}}x(t)
\end{aligned} \tag{19}$$

Remark 1. *In (16), the proposed attack model captures the key elements of stochastic deception attacks in networked contexts. The random incidence of cyber intrusions is modeled by the Bernoulli variable $\delta(t)$. The switching mechanism works as follows:*

1. *Normal Transmission ($\delta(t)=0$): The actuators get the clean output feedback control signal $K\hat{x}(t)$ while the communication channel is safe.*
2. *Active Attack ($\delta(t)=1$): An adversary injects a harmful signal after breaking through the network layer. By introducing a delayed, nonlinear distortion component $Kg(x(t-\phi(t)))$ back into the system loop, the attacker employs a complex deception approach in place of simple noise.*

In contrast to denial-of-service attacks, which interfere with data flow, deception attacks trick the controller by substituting fake information for authentic signals. The network-induced transmission delays $\phi(t)$ that an attacker must deal with while intercepting and altering packets are reflected in the malicious term $g(x(t-\phi(t)))$, which makes use of delayed state information. A sector condition bounds the nonlinear function $g(\cdot)$, preventing unlimited malicious energy, imposing realistic restrictions on the attacker's signal size, and preserving analytical tractability for the extended dissipativity study.

Remark 2. *The adaptive threshold $v(t)$ in the event-triggered condition is not a static constant but a dynamic variable governed by the differential law: $\dot{v}(t) = \left(\frac{1}{v^2(t)} - \frac{v_0}{v(t)}\right)e^T(t)He(t)$. From a control perspective, this law ensures that when the synchronization error $e(t)$ is large (e.g., during the initial phase or during a deception attack), $\dot{v}(t)$ decreases, thereby tightening the triggering condition. This forces a higher sampling frequency to suppress the error. Conversely, as the error $e(t) \to 0$, the threshold $v(t)$ relaxes to conserve communication bandwidth. This dynamic adaptation is critical for balancing the H_∞ disturbance attenuation level γ against the average inter-event time.*

Assumption 2. *The matrices Φ_1, Φ_2, Φ_3, and Φ_4 satisfy the following conditions:*

1. $\Phi_1 = \Phi_1^T \leq 0$, $\Phi_3 = \Phi_3^T > 0$, $\Phi_4 = \Phi_4^T \geq 0$,
2. $(\|\Phi_1\| + \|\Phi_2\|)\Phi_4 = 0$.

Definition 1 ([4]). *The system (19) is extended dissipative when there exist matrices $\Phi_1 \leq 0$, Φ_2, $\Phi_3 > 0$, $\Phi_4 \geq 0$ that produce the following result for all $t_f \geq 0$ and zero initial conditions.*

$$\int_0^{t_f} \left[y^T(t)\Phi_1 y(t) + 2y^T(t)\Phi_2 w(t) + w^T(t)\Phi_3 w(t) \right] dt \geq \sup_{0 \leq t \leq t_f} y^T(t)\Phi_4 y(t). \tag{20}$$

Definition 2 ([5]). *The system (19) allows the existence of a positive scalar $v > 0$ that satisfies the condition when the time derivative of the Lyapunov function meets the specified inequality*

$$\dot{\mathbb{V}}(t) \leq -v\|x(t)\|^2, \tag{21}$$

where $\|x(t)\|^2 = x^T(t)x(t)$, therefore (19) with $w(t) = 0$ satisfies quadratic stability.

Lemma 1 ([6]). *The following inequality holds for all continuously differentiable functions ω in $[a, b] \to \mathbb{R}^p$ when $R > 0$ is selected as the matrix.*

$$\int_a^b \dot{\omega}^T(u) R \dot{\omega}(u)\, du \geq \frac{1}{b-a}\Omega_0^T R \Omega_0 + \frac{3}{b-a}\Omega_1^T R \Omega_1,$$

where $\Omega_0 = \omega(b) - \omega(a)$, $\Omega_1 = \omega(b) + \omega(a) - \frac{2}{b-a}\int_a^b \omega(u)\, du$.

Lemma 2 ([7]). *The function $\Theta(\alpha, R)$ is defined for all vectors $\xi \in \mathbb{R}^q$ through the parameters α which belongs to $(0, 1)$ and the positive matrix $R \in \mathbb{R}^p$ and the two matrices W_1 and $W_2 \in \mathbb{R}^{p \times q}$, then*

$$\Theta(\alpha, R) = \frac{1}{\alpha}\xi^T W_1^T R W_1 \xi + \frac{1}{1-\alpha}\xi^T W_2^T R W_2 \xi.$$

Then, if a matrix $X \in \mathbb{R}^{p \times q}$ exists such that $\begin{bmatrix} R & X \\ * & R \end{bmatrix} > 0$, the subsequent inequality satisfies: $\min_{\alpha \in (0,1)} \Theta(\alpha, R) \geq \begin{bmatrix} W_1\xi \\ W_2\xi \end{bmatrix}^T \begin{bmatrix} R & X \\ * & R \end{bmatrix} \begin{bmatrix} W_1\xi \\ W_2\xi \end{bmatrix}$.

Lemma 3 ([8]). *The system (19) requires the introduction of a time-dependent delay function $\eta(t)$. Let $Q_1 \in \mathcal{S}^{4n}$, $\mathcal{N}_i \in \mathcal{S}^{2n}$, $i = 1, 2$, and $x : \mathbb{R} \to \mathbb{R}^n$ be a differentiable function, such that x is integrable. The function works with any matrices $\mathcal{L}_1, \mathcal{M}_1 \in \mathbb{R}^{m \times 7n}$, $\mathcal{L}_2, \mathcal{M}_2 \in \mathbb{R}^{m \times n}$, $m \in \mathbb{R}$ changeable, and any vector $\zeta_g \in \mathbb{R}^m$, if*

$$Q_{\mathcal{N}1} = Q_1 + Sym\{\mathcal{E}_{r2}^T \mathcal{N}_1 \mathcal{E}_{r3}\} \geq 0, \tag{22}$$

$$Q_{\mathcal{N}2} = Q_1 + Sym\{\mathcal{E}_{r2}^T \mathcal{N}_2 \mathcal{E}_{r3}\} \geq 0, \tag{23}$$

the following inequality holds:

$$\begin{aligned} &-\eta \int_{t-\eta}^{t} x_4^T(s,t) Q_1 x_4(s,t)\, dv \\ &\leq \eta\{x_7^T(t,t)\mathcal{N}_1 x_7(t,t) - x_7^T(t-\eta,t)\mathcal{N}_2 x_7(t-\eta,t) - x_7^T(t-\eta(t),t) \\ &(\mathcal{N}_1 - \mathcal{N}_2)x_7(t-\eta(t),t)\} + Sym\{\zeta_g^T \mathcal{L}\zeta_{Q1} + \zeta_g^T \mathcal{M}\zeta_{Q2}\} \\ &+ \frac{\eta(t)}{\eta}\zeta_g^T \hat{\mathcal{L}}\hat{Q}_{\mathcal{N}1}^{-1}\hat{\mathcal{L}}^T\zeta_g + \frac{\eta - \eta(t)}{\eta}\zeta_g^T \hat{M}\hat{Q}_{\mathcal{N}2}^{-1}\hat{M}^T\zeta_g, \end{aligned} \tag{24}$$

where

$$\begin{aligned}
x_7(t,t) &= \mathcal{E}_1\zeta(t), \quad x_7(t-\eta(t),t) = \mathcal{E}_2\zeta(t), \quad x_7(t-\eta,t) = \mathcal{E}_3\zeta(t),\\
\zeta_{Q1} &= \mathcal{E}_4\zeta(t), \quad \zeta_{Q2} = \mathcal{E}_5\zeta(t),\ \mathcal{L} = [\mathcal{L}_1,\mathcal{L}_2], \quad \mathcal{M} = [\mathcal{M}_1,\mathcal{M}_2],\\
\mathcal{E}_{r2} &= col\{\hat{\jmath}_3,\hat{\jmath}_4\}, \quad \mathcal{E}_{r3} = col\{\hat{\jmath}_1,\hat{\jmath}_2+\hat{\jmath}_3\},\\
\mathcal{E}_1 &= col\{\jmath_1,\eta\jmath_1\}, \quad \mathcal{E}_2 = col\{\jmath_2,\jmath_{12}\}, \quad \mathcal{E}_3 = col\{\jmath_3,0\},\\
\hat{\mathcal{L}} &= [\mathcal{L}_1,0_{m\times n},\mathcal{L}_2,0_{m\times 3n}], \quad \hat{\mathcal{M}} = [\mathcal{M}_1,0_{m\times n},\mathcal{M}_2,0_{m\times 3n}],\\
\hat{\mathcal{Q}}_{\mathcal{N}1} &= diag\{\mathcal{Q}_{\mathcal{N}1},3\mathcal{Q}_{\mathcal{N}1},5\mathcal{Q}_{\mathcal{N}1}\}, \quad \hat{\mathcal{Q}}_{\mathcal{N}2} = diag\{\mathcal{Q}_{\mathcal{N}2},3\mathcal{Q}_{\mathcal{N}2},5\mathcal{Q}_{\mathcal{N}2}\},\\
\mathcal{E}_4 &= col\{\jmath_1-\jmath_2,\eta\jmath_1-(\eta-\sigma(t))\jmath_2-\eta(t)\jmath_4,\eta(t)\jmath_4,\eta(t)\jmath_{10}\\
&\quad +(\eta-\eta(t))\jmath_8,\jmath_1+\jmath_2-2\jmath_4,\eta\jmath_1-(\eta-\eta(t))\jmath_2-4\eta(t)\jmath_6,\\
&\quad \eta(t)(2\jmath_6-\jmath_4),\jmath_1-\jmath_2+6\jmath_4-12\jmath_6\},\\
\mathcal{E}_5 &= col\{\jmath_2-\jmath_3,(\eta+\eta(t))(\jmath_2-\jmath_5),(\eta+\eta(t))\jmath_5,(\eta+\eta(t))\jmath_{11},\\
&\quad \jmath_2+\jmath_3-2\jmath_5,(\eta+\eta(t))(\jmath_2-4\jmath_7),(\eta+\eta(t))(2\jmath_7-\jmath_5),\\
&\quad \jmath_2-\jmath_3+6\jmath_5-12\jmath_7\},\jmath_i = [0_{n\times(i-1)n},I_n,0_{n\times(22-i)n}],\ i=1,2,\ldots,22.
\end{aligned}$$

Remark 3. *This framework encompasses H_∞ performance ($\Phi_1=-I$, $\Phi_2=0$, $\Phi_3=\gamma^2 I$, $\Phi_4=0$), L_2-L_∞ performance ($\Phi_1=0$, $\Phi_2=0$, $\Phi_3=\gamma^2 I$, $\Phi_4=I$), passivity ($\Phi_1=0$, $\Phi_2=I$, $\Phi_3=\gamma I$, $\Phi_4=0$), and (Q, S, R)-dissipativity ($\Phi_1=-0.5I$, $\Phi_2=I$, $\Phi_3=7I-\gamma I$, $\Phi_4=0$).*

Problem 1. *Consider the closed-loop delayed anti-synchronization error system described in (5) under cyber deception attacks. Design a hybrid-triggered controller $\mathcal{U}(t)$ so that three goals are met, at least in the sense of quadratic stability and performance.*

- *Construct a new LKF, together with network delay $\varphi(t)$ and state delay $\eta(t)$, to ensure quadratic stability of the system when the disturbance term is turned off, i.e., w(t) = 0.*
- *Develop a co-designed hybrid-triggered control rule. This controller should alternate between periodic sampling mode and an event-triggered mechanism, not always in the same way. The hybrid logic needs to keep synchronization while simultaneously suppressing or filtering out the malicious deception attacks (the cyber deception parts).*
- *Create a solvable LMIs framework that achieves extended dissipativity under disturbances $w(t)$ with a designed gain $K = Z^{-1}Y$ by decoupling the product terms of the Lyapunov variables and control gains.*

4. Main Results

This section describes the construction of an event-triggered controller for the anti-synchronization error system (19). Initially, the extended dissipative conditions of the suggested error system are derived.

$$\begin{aligned}
\xi(t) &= \mathrm{col}\Big[x(t),x(t-\eta(t)),\ x(t-\eta),\ \nu_1(t),\ \nu_2(t),\ \nu_3(t),\ \nu_4(t),\ \nu_5(t),\ \nu_6(t),\ \nu_7(t),\\
&\quad \nu_8(t),\ \nu_9(t),\ \xi_1(t),\ \dot{x}(t),\hat{\mathcal{F}}(x(t)),\hat{\mathcal{F}}(x(t-\eta(t))),g(x(t-\phi(t))),e(t),w(t)\Big],\\
G_{11} &= \begin{bmatrix}G_1\\G_2\end{bmatrix},\ G_{22} = \begin{bmatrix}G_3\\G_4\end{bmatrix}, x_1(s,t) = col\{\dot{x}(s),(s-t+\eta)\dot{x}(s),x(s),(s-t+\eta)x(s)\},\\
\xi_1(t) &= \{x(t-\phi(t)),x(t-\phi_2),\frac{1}{\phi(t)}\int_{t-\phi(t)}^{t}x(s)\,ds,\frac{1}{\phi_2-\phi(t)}\int_{t-\phi_2}^{t-\phi(t)}x(s)\,ds\},\\
e_h &= -\hat{\mathcal{A}}e_1+\hat{\mathcal{B}}e_{18}+\hat{\mathcal{C}}e_{19}+(1-\hat{\delta})K[\hat{\varepsilon}e_{13}+(1-\hat{\varepsilon}[e_{13}-e_{19}]]\\
&\quad +\hat{\delta}K\,e_{20}+\hat{H}_1e_{22}.
\end{aligned}$$

Theorem 1. *For given scalars* $0 \leq \eta(t) \leq \eta$, $0 \leq \phi(t) \leq \phi_2$, $\hat{\delta}$, v_2, $\hat{\varepsilon}$, *and matrix* K, *and matrices* $\Phi_1, \Phi_2, \Phi_3, \Phi_4$ *satisfying Assumption 2, the system described by (19) is extended dissipative, if there exist positive definite symmetric matrices* P, Q_2, Q_4, Q_5, $Q \in \mathcal{S}_+^{4n}$, $\mathcal{L}_1, \mathcal{M}_1 \in \mathbb{R}^{11m\times 7n}$, $\mathcal{L}_2, \mathcal{M}_2 \in \mathbb{R}^{11m\times n}$, $\mathcal{N}_i \in \mathcal{S}^{2n}$, $i = 1,2$, *diagonal matrices* $M_!, M_2 > 0$, *then the subsequent LMIs satisfies*

$$\begin{bmatrix} \hat{\Xi}_{[\eta(t)=0]} & \mathcal{E}_g^T \hat{\mathcal{M}} \\ * & -Q_{N2} \end{bmatrix} < 0, \tag{25}$$

$$\begin{bmatrix} \hat{\Xi}_{[\eta(t)=\eta]} & \mathcal{E}_g^T \hat{\mathcal{L}} \\ * & -Q_{N1} \end{bmatrix} < 0, \tag{26}$$

$$P - \hat{\mathcal{D}}^T \Phi_4 \hat{\mathcal{D}} \geq 0. \tag{27}$$

where $\hat{\Xi} = \Xi_{ij} + \tilde{\Xi}$

$$\begin{aligned}
\Xi_{11} &= e_1^T P e_{18} + e_{18}^T P^T e_1,\ \Xi_{12} = e_1^T Q_2 e_1 - e_3^T Q_2 e_3,\\
\Xi_{13} &= \eta^2 \mathcal{H}_{12}^T Q_1 \mathcal{H}_{12} + \eta\left\{\mathcal{E}_1^T \mathcal{N}_1 \mathcal{E}_1 - \mathcal{E}_3^T \mathcal{N}_2 \mathcal{E}_3 - \mathcal{E}_2^T(\mathcal{N}_1 - \mathcal{N}_2)\mathcal{E}_2\right\}\\
&\quad + Sym\{\mathcal{E}_g^T(\mathcal{L}\mathcal{E}_4 + \mathcal{M}\mathcal{E}_5)\} + \mathcal{E}_g^T\left[\frac{\eta(t)}{\eta}\hat{\mathcal{L}} Q_{N1}^{-1}\hat{\mathcal{L}}^T + \frac{\eta - \eta(t)}{\eta}\hat{\mathcal{M}} Q_{N2}^{-1}\hat{\mathcal{M}}^T\right]\mathcal{E}_g\\
\Xi_{14} &= \phi_2 e_{18}^T Q_4 e_{18} - \frac{1}{\phi_2}\begin{bmatrix} G_{11} \\ G_{22}\end{bmatrix}^T \bar{R}\begin{bmatrix} G_{11} \\ G_{22}\end{bmatrix},\ \Xi_{15} = e_1^T Q_5 e_1 - e_{14}^T Q_5 e_{14},\\
\Xi_{16} &= 2[-e_{17}^T Z e_{17} - e_1^T Z e_{17} - e_{17}^T Z\hat{\mathcal{A}} e_1 - e_1^T Z\hat{\mathcal{A}} e_1 + e_{17}^T Z\hat{\mathcal{B}} e_{18}\\
&\quad + e_1^T Z\hat{\mathcal{B}} e_{18} + e_{17}^T Z\hat{\mathcal{C}} e_{19} + e_1^T Z\hat{\mathcal{C}} e_{19} + (1 - \delta(t))(e_{17}^T Z K e_{13}\\
&\quad - e_{17}^T Z K(1 - \varepsilon(t)) e_{21} + e_1^T Z K e_{13} - e_1^T Z K(1 - \varepsilon(t)) e_{21})\\
&\quad + \delta(t)(e_{17}^T Z K e_{20} + e_1^T Z K e_{20}) + e_{17}^T Z\hat{H}_1 e_{22} + e_1^T Z\hat{H}_1 e_{22}],\\
\tilde{\Xi} &= -e_1^T\hat{\mathcal{D}}^T\Phi_1\hat{\mathcal{D}} e_1 - e_1^T\hat{\mathcal{D}}^T\Phi_2 e_{22} - e_{22}^T\Phi_3 e_{22} - e_{18}^T M_1 e_{18} + e_1^T\hat{\Gamma} M_1\hat{\Gamma} e_1,\\
&\quad - e_{19}^T M_2 e_{19} + e_2^T\hat{\Gamma} M_2\hat{\Gamma} e_2 + e_{21}^T(1 - v_2) H e_{21} - e_{20}\hat{\delta} I e_{20}.
\end{aligned}$$

Proof. There are four steps in the proof outline. To capture the second-order inertial dynamics, time-varying state delay $\eta(t)$, and hybrid-triggered sampling intervals $\phi(t)$, a delay-dependent LKF is first built. Second, in order to manage the integral terms without being excessively conservative, its time derivative is calculated along the error trajectories and strictly bounded using Lemmas 1 and 3. Third, activation nonlinearities and precise system dynamics are taken into consideration by including a zero-equation and Lipschitz sector limitations. The resultant equation is then put together into a quadratic form and transformed into the tractable LMIs (23)–(25), which provide extended dissipativity and quadratic stability, using the Schur complement.

First, to prove the system (19) is quadratically stable, the following LKF is constructed:

$$V(t) = \sum_{i=1}^{5} V_i(t), \tag{28}$$

where

$$
\begin{aligned}
V_1(t) &= x^T(t)Px(t),\\
V_2(t) &= \int_{t-\eta}^{t} x^T(s)Q_2x(s)\,ds,\\
V_3(t) &= \eta\int_{t-\eta}^{t}(s-t+\eta)x_1^T(s,t)Qx_1(s,t)\,ds,\\
V_4(t) &= \int_{t-\phi_2}^{t}\int_{s}^{t}\dot{x}^T(v)Q_4\dot{x}(v)\,dv\,ds,\\
V_5(t) &= \int_{t-\phi_2}^{t} x^T(s)Q_5x(s)\,ds.
\end{aligned}
$$

The time derivatives of the LKF components V_i $(i = 1,2,3,4,5)$ are given as follows:

$$\dot{V}_1 = 2x^T(t)P\dot{x}(t) = \xi^T(t)\Xi_{11}\xi(t), \tag{29}$$

$$\dot{V}_2 = x^T(t)Q_2x(t) - x^T(t-\eta)Q_2x(t-\eta) = \xi^T(t)\Xi_{12}\xi(t), \tag{30}$$

$$\dot{V}_3 = \eta^2x_1^T(t,t)Qx_1(t,t) - \eta\int_{t-\eta}^{t} x_1^T(s,t)Qx_1(s,t)\,ds. \tag{31}$$

Next to bound the Q-dependent integral term in (31). The Lemma 2 to this integral term with the parameterization of ζ_g as $E_g\zeta(t)$ establishes that the following inequality holds when both positive-definiteness conditions (17) and (18) are fulfilled.

$$-\eta\int_{t-\eta}^{t} x_1^T(s,t)Qx_1(s,t)\,ds \le \xi^T(t)\Pi_3(\eta(t))\xi(t) + \Pi(\eta(t)), \tag{32}$$

where

$$
\begin{aligned}
\Pi(\eta(t)) &= \zeta^T(t)\mathcal{E}_g^T\left[\frac{\eta(t)}{\eta}\hat{\mathcal{L}}Q_{N1}^{-1}\hat{\mathcal{L}}^T + \frac{\eta-\eta(t)}{\eta}\hat{\mathcal{M}}Q_{N2}^{-1}\hat{\mathcal{M}}^T\right]\mathcal{E}_g\zeta(t),\\
\Pi_3(\eta(t)) &= \eta^2\mathcal{H}_{12}^TQ\mathcal{H}_{12} + \Pi_{3r}(\eta(t)),\\
\Pi_{3r}(\eta(t)) &= \eta\left\{\mathcal{E}_1^T\mathcal{N}_1\mathcal{E}_1 - \mathcal{E}_3^T\mathcal{N}_2\mathcal{E}_3 - \mathcal{E}_2^T(\mathcal{N}_1-\mathcal{N}_2)\mathcal{E}_2\right\}\\
&\quad + Sym\{\mathcal{E}_g^T(\mathcal{L}\mathcal{E}_4 + \mathcal{M}\mathcal{E}_5)\},
\end{aligned} \tag{33}
$$

$$\dot{V}_3 \le \xi^T(t)\Xi_{13}\xi(t), \tag{34}$$

where

$$
\begin{aligned}
\zeta(t) &= col\{\zeta_2(t), \nu_9(t)\},\ \nu_9(t) = (\eta-\eta(t))\,x(t-\eta(t)),\\
\zeta_2(t) &= \mathrm{col}\{\zeta_1(t), \nu_5(t), \nu_6(t), \nu_7(t), \nu_8(t)\},\\
\zeta_1(t) &= \mathrm{col}\{x(t), x(t-\eta(t)), x(t-\eta), \nu_1(t), \nu_2(t), \nu_3(t), \nu_4(t)\},\\
\nu_1(t) &= \frac{1}{\eta(t)}\int_{t-\eta(t)}^{t} x(s)\,ds,\ \nu_2(t) = \frac{1}{\eta-\eta(t)}\int_{t-\eta}^{t-\eta(t)} x(s)\,ds,\\
\nu_3(t) &= \frac{1}{\eta^2(t)}\int_{t-\eta(t)}^{t}(s-t+\eta(t))x(s)\,ds,\\
\nu_4(t) &= \frac{1}{(\eta-\eta(t))^2}\int_{t-\eta}^{t-\eta(t)}(s-t+\eta)x(s)\,ds,\\
\nu_5(t) &= \eta(t)\,\nu_1(t),\ \nu_6(t) = (\eta-\eta(t))\,\nu_2(t),\ \nu_7(t) = \eta(t)\,\nu_3(t),\\
\nu_8(t) &= (\eta-\eta(t))\,\nu_4(t),\ \mathcal{E}_g = \mathrm{col}\{\mathcal{J}_1, \mathcal{J}_8, \ldots, \mathcal{J}_{18}\},\\
\mathcal{H}_{12} &= col\{e_h,\ \eta e_h, e_1, \eta e_1\},\\
\dot{V}_4 &= \phi_2\dot{x}^T(t)Q_4\dot{x}(t) - \int_{t-\phi_2}^{t}\dot{x}^T(v)Q_4\dot{x}(v)\,dv.
\end{aligned} \tag{35}
$$

To estimate $-\int_{t-\phi_2}^{t} \dot{x}^T(v)Q_4\dot{x}(v)\,dv$, considering the influence of the time-varying network delay $\phi(t) \in [0, \phi_2]$, we apply Lemma 1. The integral is split as follows:

$$
\begin{aligned}
-\int_{t-\phi_2}^{t} \dot{x}^T(v)Q_4\dot{x}(v)\,dv &= -\int_{t-\phi(t)}^{t} \dot{x}^T(v)Q_4\dot{x}(v)\,dv - \int_{t-\phi_2}^{t-\phi(t)} \dot{x}^T(v)Q_4\dot{x}(v)\,dv,\\
-\int_{t-\phi_2}^{t} \dot{x}^T(v)Q_4\dot{x}(v)\,dv &\le -\xi^T(t)\left(\frac{1}{\phi(t)}\begin{bmatrix}G_1\\G_2\end{bmatrix}^T \bar{R}\begin{bmatrix}G_1\\G_2\end{bmatrix} + \frac{1}{\phi_2-\phi(t)}\begin{bmatrix}G_3\\G_4\end{bmatrix}^T \bar{R}\begin{bmatrix}G_3\\G_4\end{bmatrix}\right)\xi(t),\\
&\le -\xi^T(t)\left(\frac{1}{\phi_2}\begin{bmatrix}G_{11}\\G_{22}\end{bmatrix}^T \bar{R}\begin{bmatrix}G_{11}\\G_{22}\end{bmatrix}\right)\xi(t),\\
\dot{V}_4 &\le \xi^T(t)\Xi_{14}\xi(t),
\end{aligned} \tag{36}
$$

where

$$
\bar{R} = \begin{bmatrix} Q_4 & 0 & 0 & 0\\ 0 & 3Q_4 & 0 & 0\\ 0 & 0 & Q_4 & 0\\ 0 & 0 & 0 & 3Q_4 \end{bmatrix},\ G_{11} = [G_1 \quad G_2]^T,\ G_{22} = [G_3 \quad G_4]^T,
$$

$$
G_1 = [I_n, \underbrace{0,0,0,}_{12\text{ times}} -I_n, \underbrace{0,0,0,}_{8\text{ times}}], \quad G_2 = [\underbrace{0,0,0,}_{12\text{ times}} I_n, I_n, 2I_n, \underbrace{0,0,0,}_{7\text{ times}}],
$$

$$
G_3 = [\underbrace{0,0,0,}_{12\text{ times}} I_n, -I_n, \underbrace{0,0,0,}_{8\text{ times}}], \quad G_4 = [\underbrace{0,0,0,}_{12\text{ times}} I_n, I_n, 0, -2I_n, \underbrace{0,0,0,}_{6\text{ times}}],
$$

and I_n is the $n \times n$ identity matrix.

$$
\begin{aligned}
\dot{V}_5 &= x^T(t)Q_5x(t) - x^T(t-\phi_2)Q_5x(t-\phi_2),\\
\dot{V}_5 &= \xi^T(t)\Xi_{15}\xi(t).
\end{aligned} \tag{37}
$$

From the inequality (17) and Assumption 1, it follows that

$$
\begin{aligned}
&\hat{\delta}g^T(x(t-\phi(t)))g(x(t-\phi(t))) \le \hat{\delta}(Gx(t))^T Gx(t),\\
&\hat{\mathcal{F}}^T(x(t))M_1\mathcal{F}(x(t)) - x(t)^T\hat{\Gamma}M_1\hat{\Gamma}x(t) \le 0,\\
&\hat{\mathcal{F}}^T(x(t-\eta(t)))M_2\hat{\mathcal{F}}(x(t-\eta(t))) - x^T(t-\eta(t))\hat{\Gamma}M_2\hat{\Gamma}x(t-\eta(t)) \le 0
\end{aligned} \tag{38}
$$

where

$$
\hat{\Gamma} = \begin{bmatrix}\mathcal{L} & 0\\ 0 & 0\end{bmatrix}, \quad \mathcal{L} = \mathrm{diag}\{\ell_1, \ell_2, \ldots, \ell_n\}.
$$

The zero equation for the anti-synchronization error system is given by:

$$
\begin{aligned}
0 &= \nu_{ab}^T(t)Z\xi_{ab}(t) + \xi_{ab}^T(t)Z\nu_{ab}(t)\\
0 &= (\dot{x}(t)+x(t))^T Z(-\dot{x}(t) + (-\hat{\mathcal{A}}x(t) + \hat{\mathcal{B}}\hat{\mathcal{F}}(x(t)) + \hat{\mathcal{C}}\hat{\mathcal{F}}(x(t-\eta(t)))\\
&\quad + (1-\delta(t))K[\varepsilon(t)x(t-\phi(t)) + (1-\varepsilon(t))[x(t-\phi(t)) - e(t)]]\\
&\quad + \delta(t)K\,g(x(t-\phi(t))) + \hat{H}_1w(t))) + (-\dot{x}(t) + (-\hat{\mathcal{A}}x(t) + \hat{\mathcal{B}}\hat{\mathcal{F}}(x(t))\\
&\quad + \hat{\mathcal{C}}\hat{\mathcal{F}}(x(t-\eta(t))) + (1-\delta(t))K[\varepsilon(t)x(t-\phi(t))\\
&\quad + (1-\varepsilon(t))[x(t-\phi(t)) - e(t)]] + \delta(t)K\,g(x(t-\phi(t)))\\
&\quad + \hat{H}_1w(t)))^T Z(\dot{x}(t)+x(t)),\\
&= \xi^T(t)\Xi_{16}\xi(t),
\end{aligned} \tag{39}
$$

where

$$\begin{aligned}
\nu_{ab}(t) &= \dot{x}(t) + x(t),\\
\xi_{ab}(t) &= -\dot{x}(t) + (-\hat{\mathcal{A}}x(t) + \hat{\mathcal{B}}\hat{\mathcal{F}}(x(t)) + \hat{\mathcal{C}}\hat{\mathcal{F}}(x(t-\eta(t)))\\
&\quad + (1-\delta(t))K[\varepsilon(t)x(t-\phi(t)) + (1-\varepsilon(t))[x(t-\phi(t)) - e(t)]]\\
&\quad + \delta(t)K\,g(x(t-\phi(t))) + \hat{H}_1 w(t)),\\
\dot{x}(t) &= -\hat{\mathcal{A}}x(t) + \hat{\mathcal{B}}\hat{\mathcal{F}}(x(t)) + \hat{\mathcal{C}}\hat{\mathcal{F}}(x(t-\eta(t)))\\
&\quad + (1-\delta(t))K[\varepsilon(t)x(t-\phi(t)) + (1-\varepsilon(t))[x(t-\phi(t)) - e(t)]]\\
&\quad + \delta(t)K\,g(x(t-\phi(t))) + \hat{H}_1 w(t)).
\end{aligned}$$

Combining (29)–(39), with $g^T(x(t-\phi(t)))g(x(t-\phi(t))) \leq x^T(t)G^TGx(t)$, and by $J(t) = y^T(t)\Phi_1 y(t) + 2y^T(t)\Phi_2 w(t) + w^T(t)\Phi_3 w(t)$, we get

$$\dot{V}(t) - J(t) \leq \xi^T(t)\hat{\Xi}\xi(t) < 0, \tag{40}$$

where $\hat{\Xi}$ is defined in Theorem 1.

The result of LMIs shows that $\hat{\Xi} < 0$ because of the mathematical expressions between Equations (25) and (31). The presence of the negative value $\hat{\Xi}$ leads to the existence of a small positive value v_1, which satisfies the condition $\hat{\Xi} < -v_1 I$.

Given this condition, inequality (40) can be expressed in the following manner:

$$\begin{aligned}
&\dot{V}(t) - J(t) \leq -v_1\|\xi(t)\|^2 \leq -v_1\|x(t)\|^2,\\
&\dot{V}(t) \leq J(t) - v_1\|x(t)\|^2.
\end{aligned} \tag{41}$$

When considering $w(t) = 0$, then $J(t) = y^T(t)\Phi_1 y(t)$. Noticing that $\Phi_1 \leq 0$ it yields that

$$\dot{V}(t) \leq -v_1\|x(t)\|^2.$$

The system described in Equation (5) demonstrates quadratic stability according to Definition 2. The next step involves establishing the extended dissipative condition that applies to our proposed model. The definition of $\hat{\Xi}$ allows for a direct conclusion that

$$\dot{V}(t) - J(t) \leq 0.$$

Integrating both sides of the above inequality from 0 to t gives

$$\int_0^t J(\alpha)d\alpha \geq V(t) - V(0) \geq x^T(t)Px(t) + \hat{\varsigma}. \tag{42}$$

The necessary demonstration of the following relationship requires proof for all matrices Φ_1, Φ_2, Φ_3, and Φ_4, which comply with Assumption 2 requirements.

$$\int_0^{t_f} J(\alpha)d\alpha - \sup_{0<t\leq t_f} y^T(t)\Phi_4 y(t) \geq 0, \tag{43}$$

The analysis for proving Equation (20) requires two different cases, which depend on the vector Φ_4 norm value. The first situation occurs when $\|\Phi_4\| = 0$, which represents either a border condition or a trivial case. The second situation handles all situations where $\|\Phi_4\| \neq 0$. The two cases provide all necessary conditions for proving the validity of Equation (20).

First case, if $\| \Phi_4 \| = 0$, then (42) implies for any $t_f \geq 0$.

$$\int_0^{t_f} J(\alpha)d\alpha \geq x^T(t_f)P_1x(t_f) + \hat{\varsigma} \geq 0, \tag{44}$$

this signifies that Definition 1 is true. If $\| \Phi_4 \| \neq 0$, we can conclude that the matrices $\Phi_1 = 0$, $\Phi_2 = 0$ and $\Phi_3 > 0$, thus for any $t_f \geq t > 0$, we have

$$\int_0^{t_f} J(\alpha)d\alpha \geq \int_0^{t} J(\alpha)d\alpha \geq x^T(t)Px(t) + \hat{\varsigma}. \tag{45}$$

Thus, according to (27), noting the fact that

$$y^T(t)\Phi_4 y(t) = x^T(t)\mathcal{E}^T\Phi_4\mathcal{E}x(t) \leq x^T(t)Px(t) \leq \int_0^{t_f} J(\alpha)d\alpha.$$

It is clear that, for any $t \geq 0$, $t_f \geq 0$ with $t_f \geq t$.

$$\int_0^{t_f} J(\alpha)d\alpha \geq y^T(t)\Phi_4 y(t) + \hat{\varsigma}.$$

Because of this, inequality (20) is valid for every $t_f \geq 0$. The analysis of both situations, specifically the conditions $\|\Phi_4\| = 0$ and $\|\Phi_4\| \neq 0$, leads to the conclusion that the suggested system (19) satisfies the extended dissipativity condition defined in Definition 1. □

Figure 2 sketches out a detailed derivation work for creating stability criteria, from building an LKF to achieve the LMI conditions. Each matrix variable is clearly tied back to its specific analytical purpose, and it is used to deal with those time-varying delays and the hybrid triggering constraints.

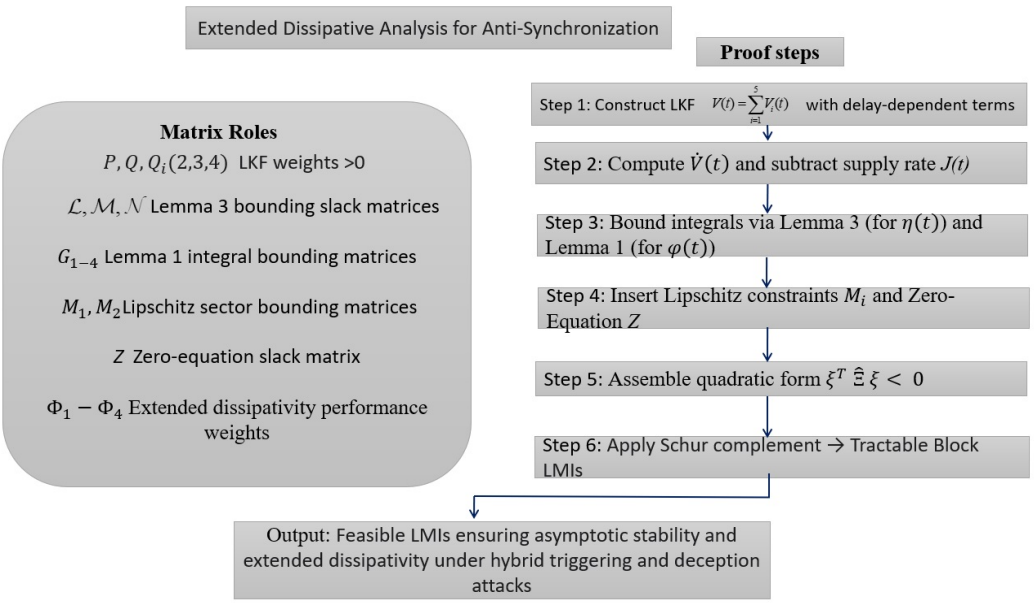

Figure 2. Road map of the derivation of the extended dissipative stability conditions.

Theorem 2. *For given scalars* $0 \leq \eta(t) \leq \eta$, $0 \leq \phi(t) \leq \phi_2$, $\hat{\delta}$, v_2, $\hat{\varepsilon}$, *and matrices* Φ_1, Φ_2, Φ_3, *and* Φ_4 *satisfying Assumption 2, the system described by (19) is extended dissipative if there exist positive definite symmetric matrices* $\tilde{P}$, $\tilde{Q}_2$, $\tilde{Q}_4$, $\tilde{Q}_5$, $\tilde{Q} \in \mathcal{S}_+^{4n}$, $\tilde{\mathcal{L}}_1, \tilde{\mathcal{M}}_1 \in \mathbb{R}^{11m\times 7n}$, $\tilde{\mathcal{L}}_2, \tilde{\mathcal{M}}_2 \in$

$\mathbb{R}^{11m\times n}$, $\tilde{\mathcal{N}}_i \in \mathcal{S}^{2n}$, $i = 1,2$, *any matrices* Y, *diagonal matrices* $\tilde{M}_1, \tilde{M}_2 > 0$, *such that the following matrix inequalities hold:*

$$\begin{bmatrix} \hat{\Xi}_{[\eta(t)=0]} & \mathcal{E}_g^T\hat{\mathcal{M}} \\ * & -Q_{N2} \end{bmatrix} < 0, \tag{46}$$

$$\begin{bmatrix} \hat{\Xi}_{[\eta(t)=\eta]} & \mathcal{E}_g^T\hat{\mathcal{L}} \\ * & -Q_{N1} \end{bmatrix} < 0, \tag{47}$$

$$\begin{bmatrix} \tilde{P} & Z\hat{\mathcal{D}}^T \\ * & \Phi_4 \end{bmatrix} > 0 \tag{48}$$

then the drive system (2) and response system (3) can achieve the synchronization, and the controller gain matrix K *is given as* $K = Y\mathcal{Z}^{-T}$.
where $\hat{\Xi} = \Xi_{ij} + \tilde{\Xi}$

$$\begin{aligned}
&\Xi_{11} = 2e_1^T\tilde{P}e_{18},\ \Xi_{12} = e_1^T\tilde{Q}_2e_1 - e_3^T\tilde{Q}_2e_3,\\
&\Xi_{13} = \eta^2\mathcal{H}_{12}^T\tilde{Q}_1\mathcal{H}12 + \eta\left\{\mathcal{E}_1^T\tilde{\mathcal{N}}_1\mathcal{E}_1 - \mathcal{E}_3^T\tilde{\mathcal{N}}_2\mathcal{E}_3 - \mathcal{E}_2^T(\tilde{\mathcal{N}}_1 - \tilde{\mathcal{N}}_2)\mathcal{E}_2\right\}\\
&\quad + Sym\{\mathcal{E}_g^T(\tilde{\mathcal{L}}\mathcal{E}_4 + \tilde{\mathcal{M}}\mathcal{E}_5)\} + \mathcal{E}_g^T\left[\frac{\eta(t)}{\eta}\hat{\mathcal{L}}Q_{N1}^{-1}\hat{\mathcal{L}}^T + \frac{\eta-\eta(t)}{\eta}\hat{\mathcal{M}}Q_{N2}^{-1}\hat{\mathcal{M}}^T\right]\mathcal{E}_g\\
&\Xi_{14} = \phi_2e_{18}^T\tilde{Q}_4e_{18} - \frac{1}{\phi_2}\begin{bmatrix}G_{11}\\G_{22}\end{bmatrix}^T\bar{R}\begin{bmatrix}G_{11}\\G_{22}\end{bmatrix},\ \Xi_{15} = e_1^T\tilde{Q}_5e_1 - e_{14}^T\tilde{Q}_5e_{14},\\
&\Xi_{16} = 2[-e_{17}^TZe_{17} - e_1^TZe_{17} - e_{17}^TZ\hat{\mathcal{A}}e_1 - e_1^TZ\hat{\mathcal{A}}e_1 + e_{17}^TZ\hat{\mathcal{B}}e_{18}\\
&\quad + e_1^TZ\hat{\mathcal{B}}e_{18} + e_{17}^TZ\hat{\mathcal{C}}e_{19} + e_1^TZ\hat{\mathcal{C}}e_{19} + (1-\delta(t))(e_{17}^TYe_{13}\\
&\quad - e_{17}^TY(1-\varepsilon(t))e_{21} + e_1^TYe_{13} - e_1^TY(1-\varepsilon(t))e_{21})\\
&\quad + \delta(t)(e_{17}^TYe_{20} + e_1^TYe_{20}) + e_{17}^TZ\hat{H}_1e_{22} + e_1^TZ\hat{H}_1e_{22}],\\
&\tilde{\Xi} = -e_1^T\hat{\mathcal{D}}^T\Phi_1\hat{\mathcal{D}}e_1 - e_1^T\hat{\mathcal{D}}^T\Phi_2e_{22} - e_{22}^T\Phi_3e_{22} - e_{18}^T\tilde{M}_1e_{18} + e_1^T\hat{\Gamma}\tilde{M}_1\hat{\Gamma}e_1,\\
&\quad - e_{19}^T\tilde{M}_2e_{19} + e_2^T\hat{\Gamma}\tilde{M}_2\hat{\Gamma}e_2 + e_{21}^T(1-v_2)\tilde{H}e_{21} - e_{20}\hat{\delta}Ie_{20}.
\end{aligned}$$

Proof. The proof follows the outline. The derivation uses the congruence transformation together with a change of variables, so the synthesis conditions get linearized. If we set $\mathcal{Z} = Z^{-1}$, then by pre-/post-multiplying the analysis inequalities from Theorem 1 with the block diagonal matrices Y_1 and Y_2, the whole coupling between the Lyapunov variables and the feedback gain gets removed, and we get the LMIs (45)–(47). Once those LMIs are in place, the controller gain follows as $K = Y\mathcal{Z}^{-T}$, computed in a straightforward way using standard convex optimization solvers. Define $\mathcal{Z} = Z^{-1}$, $\tilde{P} = \mathcal{Z}P\mathcal{Z}^T$, $\tilde{Q} = \mathcal{Z}Q\mathcal{Z}^T$, $\tilde{Q}_1 = \mathcal{Z}Q_1\mathcal{Z}^T$, $\tilde{Q}_2 = \mathcal{Z}Q_2\mathcal{Z}^T$, $\tilde{Q}_4 = \mathcal{Z}Q_4\mathcal{Z}^T$, $\tilde{Q}_5 = \mathcal{Z}Q_5\mathcal{Z}^T$, $\mathrm{Y}_1 = diag\{\underbrace{\mathcal{Z},\mathcal{Z},\mathcal{Z}}_{8\ times},\mathcal{Z},\mathcal{Z}\}$, $\mathrm{Y}_2 = diag\{\mathrm{Y}_1,\mathrm{Y}_1,\mathcal{Z},I,\mathcal{Z},\mathcal{Z},\mathcal{Z},\mathcal{Z}\}$. Pre- and post-multiplying (25) and (26) with Y_2, (27) with Z, we get (46)–(48). Thus, the proof is completed. □

Remark 4. *The transition from Theorem 1 to Theorem 2 involves a significant mathematical challenge: the presence of product terms between the Lyapunov matrix* P *and the controller gain* K. *In the derivation of Theorem 2, we employ the property that* $K = Z^{-1}Y$. *By introducing the diagonal matrices* $\tilde{M}_1, \tilde{M}_2$ *and the decoupling matrix* Z, *we transform the nonlinear matrix inequality (NMI) into a linear matrix inequality (LMI). This allows the use of interior-point methods (like the MATLAB LMI Toolbox) to find the globally optimal* K *that satisfies the extended dissipativity condition (20) without needing to pre-calculate the control gains.*

Remark 5. *Structure and Roles of Theorem 1 and Theorem 2:*
The main theoretical contributions are put together in two sequential results, which, in a manner, split stability checking from the actual controller synthesis bit.

(a) *Theorem 1 works mostly as a stability analysis criterion.*

i. *It provides sufficient conditions for the closed-loop anti-synchronization error system to be quadratically stable and to meet the required extended dissipative performance index.*

ii. *In this theorem, the controller gain K is assumed fixed, and it also explicitly brings in the time-varying state delay $\eta(t)$, the hybrid-triggered sampling mechanism, and stochastic deception attacks.*

iii. *All of this is handled using a tailored LKF and then tight integral bounding arguments, and the primary objective is to demonstrate the analytical inequality structure needed for further gain design and to verify system performance.*

(b) *Theorem 2 tackles the controller synthesis task.*

i. *The requirements in Theorem 1 cannot be simply solved because they involve bilinear terms between the gain K and the Lyapunov matrix P.*

ii. *In order to decouple these product factors and translate the analytical inequalities into strictly LMIs, Theorem 2 uses a nonsingular coordinate transformation and the change of variables $K = Z^{-1}Y$.*

iii. *This result eliminates the need for iterative tuning or pre-selection of K and allows for the direct numerical computation of the state-feedback gain using typical LMI solvers. So, together, these theorems kind of form a whole pipeline, from verification to computation: Theorem 1 checks closed-loop performance assuming the control parameters are already known, while Theorem 2 provides a numerically friendly route to synthesize a controller gain that preserves the same performance targets.*

5. Simulation Results

The efficiency and robustness of the suggested control strategy are demonstrated by the presentation of the numerical example under the extended dissipative framework and deception attacks for verification goals.

Consider a 2-neuron states $x_i(t), i \in \mathbb{N}_2$ delayed INNs (19) and the following parameters are given

$$\aleph = \begin{bmatrix} 2.2 & 0 \\ 0 & 2.2 \end{bmatrix}, \mathcal{A} = \begin{bmatrix} 2 & 0 \\ 0 & 2 \end{bmatrix}, \mathcal{B} = \begin{bmatrix} -1.1 & 0.2 \\ 0.3 & 0.5 \end{bmatrix}, \mathcal{C} = \begin{bmatrix} 1.2 & -0.2 \\ 0.5 & -0.2 \end{bmatrix},$$
$$g_j(y_j) = \frac{1 - e^{-\tilde{y}_j}}{1 + e^{-\tilde{y}_j}}, \quad j = 1, 2, \ \mathcal{H}_1 = \begin{bmatrix} 1.2 & 0 \\ -0.3 & 0.2 \end{bmatrix}, \mathcal{D} = \begin{bmatrix} 0.2 & 0 \\ 0 & 0.2 \end{bmatrix}.$$

and the time-varying delay is defined as $\eta(t) = 0.5\sin^2(t)$. Since $\sin^2(t) \in [0, 1]$, it follows that $0 \leq \eta(t) \leq 0.5$, which implies that the upper bound of the delay is $\eta_1 = 0.5$. Moreover, $\dot{\eta}(t) = 0.5\sin(2t)$, leading to $|\dot{\eta}(t)| \leq 0.5$. Therefore, the chosen delay function satisfies the bounded conditions $0 \leq \eta(t) \leq \eta_1$ and $|\dot{\eta}(t)| \leq \mu$, where $\eta_1 = 0.5$ and $\mu = 0.5$. Then, we can obtain the corresponding matrices of system (19) as follows:

$$\hat{\mathcal{A}} = \begin{bmatrix} 1 & 0 & -1 & 0 \\ 0 & 1 & 0 & -1 \\ 0.8 & 0 & 1.2 & 0 \\ 0 & 0.8 & 0 & 1.2 \end{bmatrix}, \hat{\Gamma} = \begin{bmatrix} 0.67 & 0 & 0 & 0 \\ 0 & 0.67 & 0 & 0 \\ 0 & 0 & 0 & 0 \\ 0 & 0 & 0 & 0 \end{bmatrix},$$

$$\hat{\mathcal{B}} = \begin{bmatrix} 0 & 0 & 0 & 0 \\ 0 & 0 & 0 & 0 \\ -1.1 & 0.2 & 0 & 0 \\ 0.3 & 0.5 & 0 & 0 \end{bmatrix}, \hat{\mathcal{C}} = \begin{bmatrix} 0 & 0 & 0 & 0 \\ 0 & 0 & 0 & 0 \\ 1.2 & -0.2 & 0 & 0 \\ 0.5 & -0.2 & 0 & 0 \end{bmatrix},$$

$$\hat{H}_1 = \begin{bmatrix} \mathcal{H}_{\delta 1} & \mathcal{H}_{\delta 2} \end{bmatrix}, \mathcal{H}_{\delta 1} = \begin{bmatrix} 0 & 0 & 1.2 & -0.3 \end{bmatrix}^T,$$

$$\mathcal{H}_{\delta 2} = \begin{bmatrix} 0 & 0 & 0 & 0.2 \end{bmatrix}^T, g_j(y_j) = \frac{1 - e^{-\tilde{y}_j}}{1 + e^{-\tilde{y}_j}}, \quad j = 1, 2.$$

For the different values of η, the sampling upper bounds ϕ_2 are calculated as shown in Table 1.

Table 1. Comparison of ϕ_2 for different values of η.

η	0.01	0.02	0.03	0.05	0.08
ϕ_2	0.2955	0.2617	0.1386	0.1542	0.1634

Through solving the LMI constraints outlined in Theorem 2, we obtained feasible solutions and control gain matrices for various extended dissipativity performance cases, confirming the effectiveness of the proposed event-triggered control strategy. Four distinct extended dissipative scenarios were analyzed and simulated using MATLAB 2021 LMI Toolbox.

We select the external disturbance $w(t) = 0.3e^{-0.8t}sin(5t)$ and we add its associated weighting matrices Φ_1, Φ_2, Φ_3, and Φ_4 to Table 2. The extended dissipative condition becomes achievable through parameter application and LMIs solution methods that Theorem 2 provides, together with the MATLAB LMI toolbox. The condition requires four cases, which include (i) passivity, (ii) (Q, S, R)- dissipativity, (iii) H_∞ case, and (iv) $L_2 - L_\infty$ performance as a singular instance.

Table 2. Matrices for every behavior in the extended dissipative scenario.

Analysis	$\mathbf{\Phi_1}$	$\mathbf{\Phi_2}$	$\mathbf{\Phi_3}$	$\mathbf{\Phi_4}$
Passivity	0	I	γI	0
(Q, S, R)-dissipativity	$-0.5I$	I	$I - \beta I$	0
H_∞	$-I$	0	$\gamma^2 I$	0
$L_2 - L_\infty$	0	0	$\gamma^2 I$	I

Feasibility results:

(i) Choosing $\Phi_1 = 0, \Phi_2 = I, \Phi_3 = \gamma I, \Phi_4 = 0$, and $\hat{\varsigma} = 0$, the extended dissipativity performance of the anti-synchronized INNs reduced to a passivity condition. The corresponding control gain matrix is obtained as $K = \begin{bmatrix} 1.5263 & 0.2012 & 0.0245 & 0.1202 \\ 0.0021 & -2.1453 & 0.1845 & 0.0125 \\ 0.1257 & 0.2457 & -2.5687 & 0.0897 \\ 0.0378 & 0.0782 & 0.1952 & -1.2455 \end{bmatrix}$.
Furthermore, the minimum passivity performance index γ is estimated as 2.4123.

Passivity case (No attack): The closed-loop system performance under passive control without deception attacks is shown in Figure 3. After a short transient, the error states

$x(t)$ converges to zero in subplot (a) and the inset shows an enlarged view of curves from t = [2, 8]. In subplot (b), the bounded control inputs $\mathcal{U}(t)$ stabilize the system and the inset shows an enlarged view of curves from t = [1, 6]. Subplot (c) shows stable phase trajectories convergent to the origin in the ϖ_1–$\wp_1$ plane from the initial state (red circle). The adaptive evolution of the threshold parameter $\phi(t)$ is shown in subplot (d). In subplot (e), the error norm $|x(t)|$ gradually decreases and remains negligible. Finally, subplot (f) shows event-triggered instants and variable intervals h_k, confirming reduced communication.

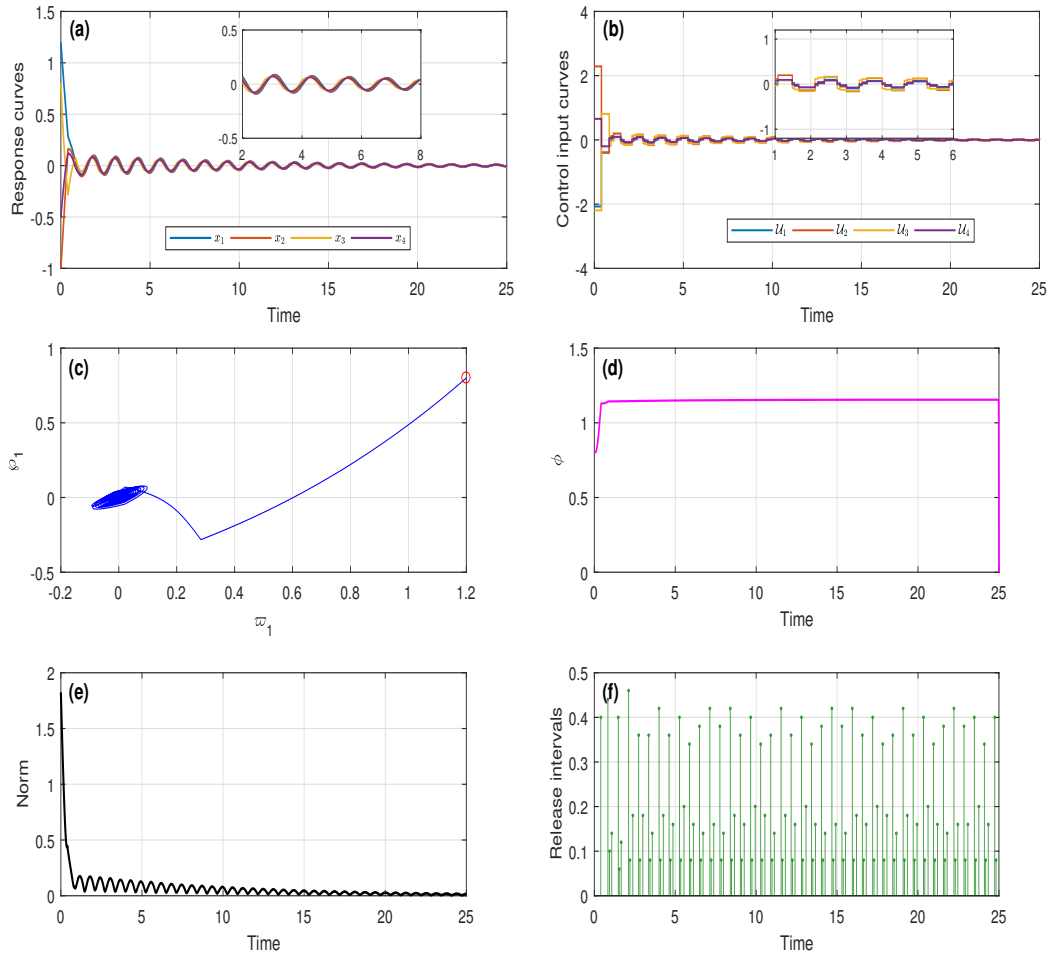

Figure 3. Passivity performance of without attack state responses, control inputs, phase portrait, adaptive threshold response, error norm, and triggered release intervals.

With attack: Figure 4 displays the system response during passive control with deception attacks at $\hat{\delta} = 0.2$. In subplot (a), attacks cause small variations as error states converge to zero. The control inputs in (b) vary briefly but remain stable. Subplot (c) shows steady phase trajectories near the origin from the initial state (red circle). (d) shows the adaptive behavior of the threshold parameter $\phi(t)$. The error norm $|x(t)|$ decays with time in (e) despite short-term perturbations. Finally, subplot (f) shows event-triggered instants with different intervals h_k, showing how well communication works under attack.

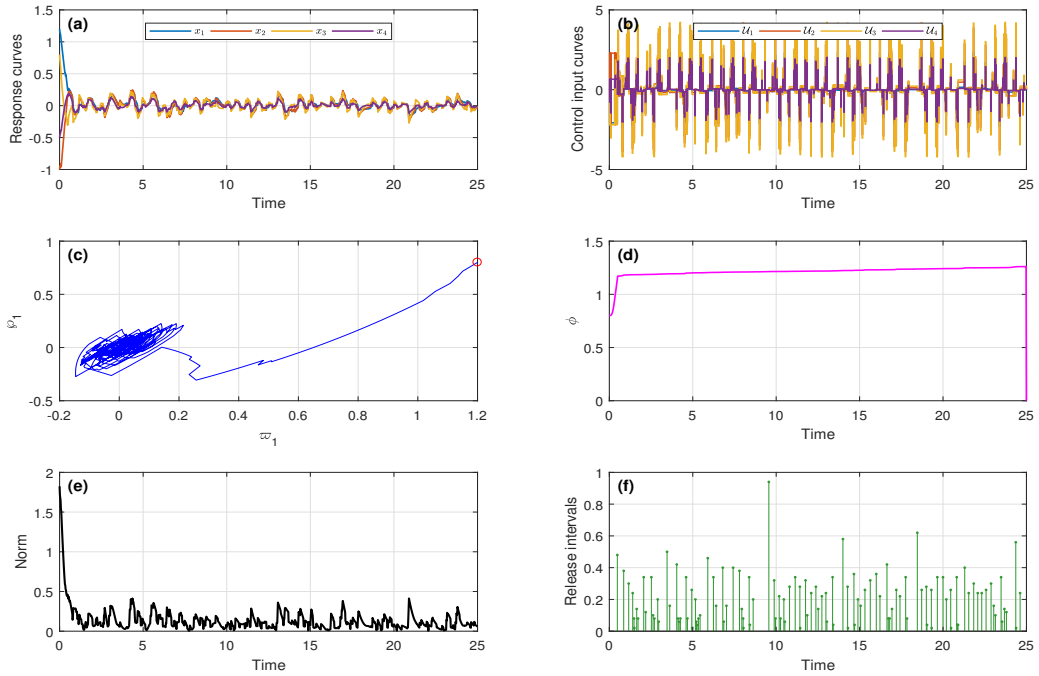

Figure 4. Passivity performance of with attack state responses, control inputs, phase portrait, adaptive threshold response, error norm, and triggered release intervals.

(ii) The extended dissipativity condition in Definition 1 is deduced to (Q, S, R)-dissipative performance for the matrices $\Phi_1 = -0.5I$, $\Phi_2 = I$, $\Phi_3 = I - \beta * I, \Phi_4 = 0$, and $\hat{\varsigma} = 0$. By solving the LMIs in Theorem 2, the prescribed gain matrix is deduced as $K = \begin{bmatrix} 4.5263 & 0.5012 & 0.1245 & 0.3202 \\ 0.1021 & -5.1453 & 0.4845 & 0.2125 \\ 0.4257 & 0.5457 & -6.5687 & 0.3897 \\ 0.1378 & 0.2782 & 0.4952 & -4.2455 \end{bmatrix}$ along with maximum dissipative index γ as 4.3214.

(Q, S, R)-dissipativity case (No attack): Figure 5 shows system performance without attacks under (Q, S, R)-dissipativity management. Within subplot (a), the error states $x(t)$ rapidly falls to zero. (b) has smooth, well-regulated control inputs. Subplot (c) reveals stable phase trajectories approaching the origin from the initial state (red circle). Figure 5d shows the adaptive evolution of the threshold $\phi(t)$. In (e), the error norm $|x(t)|$ rapidly decreases and remains negligible. Last, subplot (f) shows trigger instants and varying intervals, proving effective communication reduction.

With attack: Figure 6 shows the (Q, S, R)-dissipative response to deception attacks with $\hat{\delta} = 0.2$. The error states $x(t)$ converges to zero with relatively small oscillations in subplot (a). The control inputs in (b) increase briefly during attacks but stabilize. Subplot (c) shows steady phase trajectories near the origin from the initial state (red circle). The adaptive evolution of $\phi(t)$ is depicted in (d). Even with short-term increases, the error norm decays in (e). Finally, subplot (f) shows trigger instants and varying intervals, showing persistent communication efficiency under attacks.

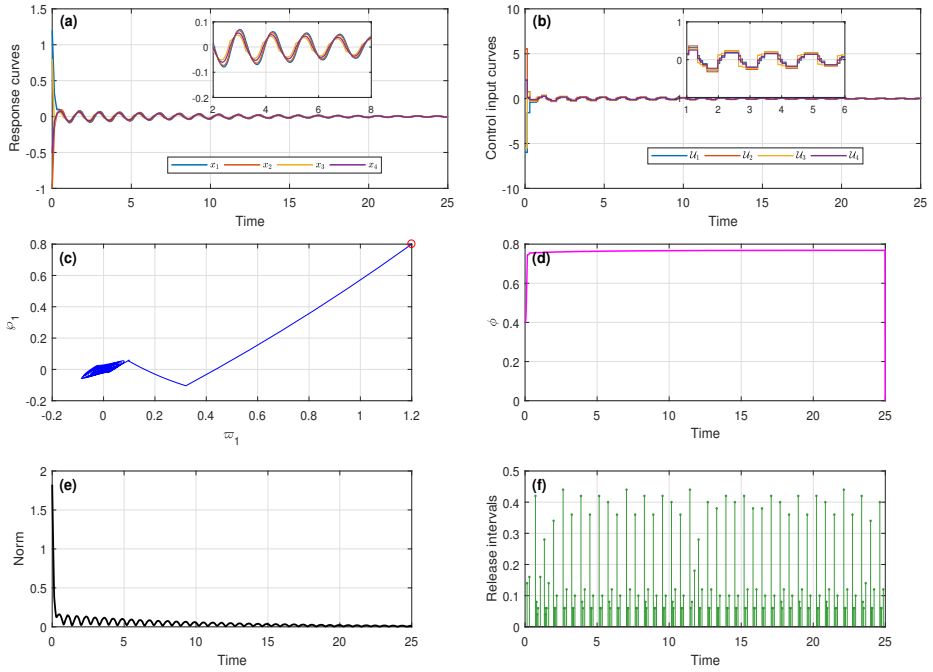

Figure 5. (Q, S, R)-dissipative performance of without attack state responses, control inputs, phase portrait, adaptive threshold response, error norm, and triggered release intervals.

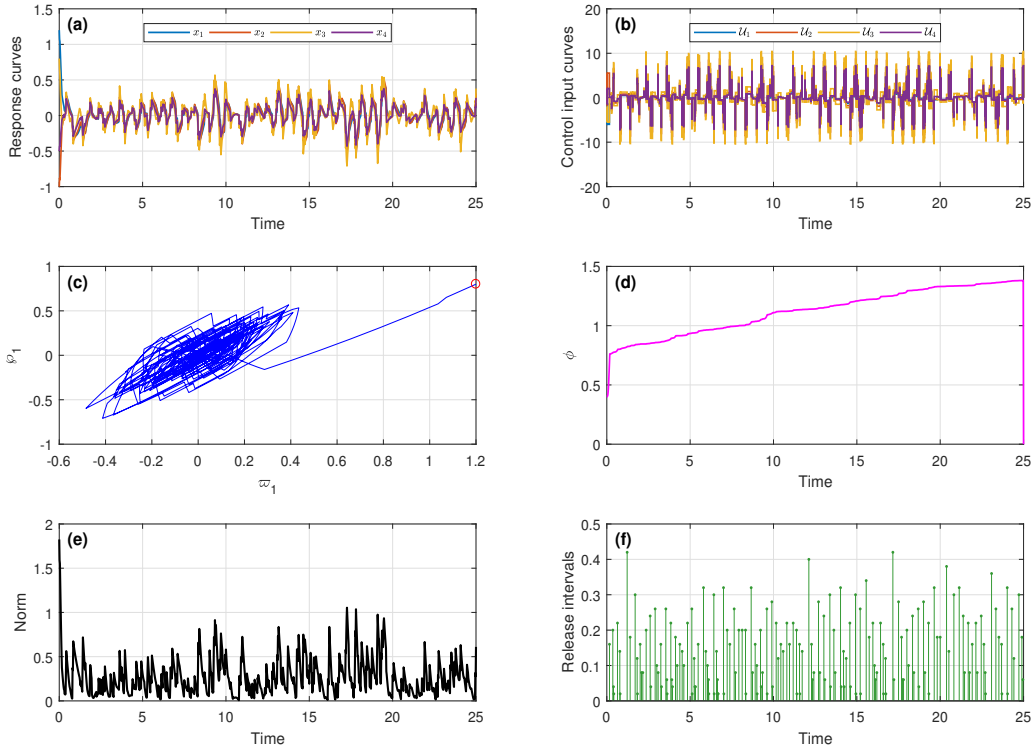

Figure 6. (Q, S, R)-dissipative performance with attack state responses, control inputs, phase portrait, adaptive threshold response, error norm, and triggered release intervals.

(iii) By setting $\Phi_1 = -I$, $\Phi_2 = 0$, $\Phi_3 = \gamma^2 I, \Phi_4 = 0$, it can be observed that the extended dissipative performance attains the H_∞ conditions together with the control gain

matrix $K = \begin{bmatrix} 1.0263 & 0.1012 & 0.0145 & 0.0202 \\ 0.0011 & -1.1453 & 0.0845 & 0.0025 \\ 0.0257 & 0.1457 & -1.5687 & 0.0397 \\ 0.0178 & 0.0282 & 0.0952 & -0.9455 \end{bmatrix}$. The corresponding minimum H_∞ performance level γ is derived as 1.2123. H_∞ case (No attack): Figure 7 shows control performance without deception attacks at H_∞. Error states $x(t)$ converges to zero in subplot (a). Bounded and well-regulated control inputs in (b). Subplot (c) reveals stable phase trajectories approaching the origin from the initial state (red circle). Subplot (d) shows the adaptive evolution of the threshold $\phi(t)$. In (e), the error norm $|x(t)|$ rapidly decreases and remains low. Finally, subplot (f) shows trigger instants and variable intervals h_k, proving communication reduction.

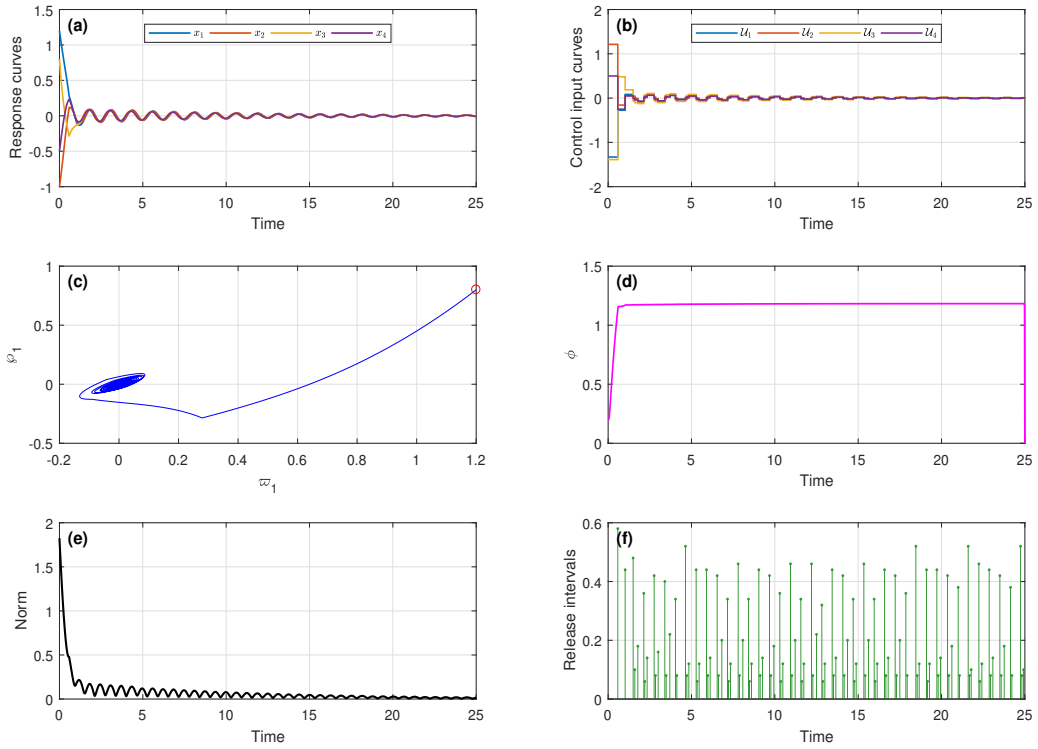

Figure 7. H_∞ performance of without attack state responses, control inputs, phase portrait, adaptive threshold response, error norm, and triggered release intervals.

With attack: Figure 8 displays H_∞ control performance under deception attacks with $\hat{\delta} = 0.2$. Subplot (a) shows error states converging near zero with modest oscillations. The control inputs in (b) vary briefly yet keep the system stable. Subplot (c) shows steady phase trajectories near the origin from the initial state (red circle). The adaptive behavior of $\phi(t)$ is seen in (d). Short-term changes do not stop the error norm from decreasing in (e). Finally, subplot (f) shows the trigger instants and variable intervals h_k, proving the hybrid event-triggered scheme's attack resistance.

(iv) $L_2 - L_\infty$ performance is obtained by choosing the matrices as $\Phi_1 = 0$, $\Phi_2 = 0$, $\Phi_3 = \gamma^2 I, \Phi_4 = I$, from which the gain matrix and performance index γ are calculated as $K = \begin{bmatrix} 6.5263 & 1.2123 & 0.5456 & 0.8024 \\ 0.5214 & -7.1453 & 1.0457 & 0.6254 \\ 0.8578 & 1.4578 & -8.5687 & 0.9975 \\ 0.5781 & 0.9821 & 1.2521 & -6.2455 \end{bmatrix}$, and 1.1204. respectively.

L_2-L_∞ case (No attack): Figure 9 shows the performance without deception attacks from L_2 to L_∞. In subplot (a), the error states $x(t)$ converges smoothly to zero. Bounded and

well-regulated control inputs in (b). Subplot (c) reveals stable phase trajectories approaching the origin from the initial state (red circle). The adaptive evolution of $\phi(t)$ is shown in (d). In (e), the error norm rapidly decreases and stays minimal. Finally, subplot (f) shows trigger instants and intervals, showing the efficient communication.

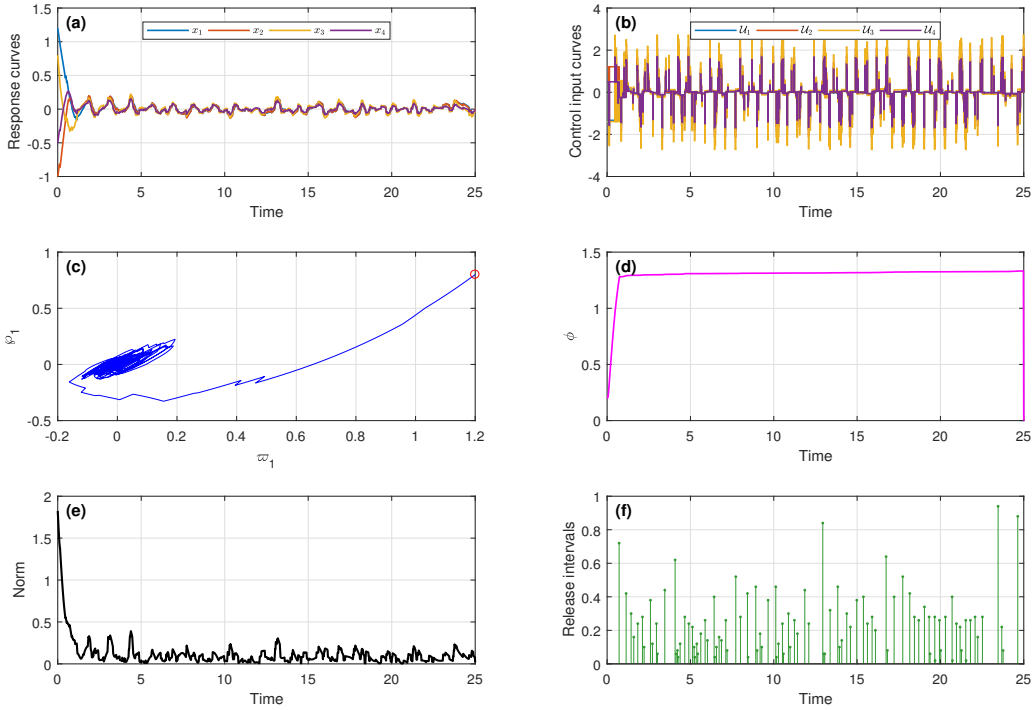

Figure 8. H_∞ performance with attack state responses, control inputs, phase portrait, adaptive threshold response, error norm, and triggered release intervals.

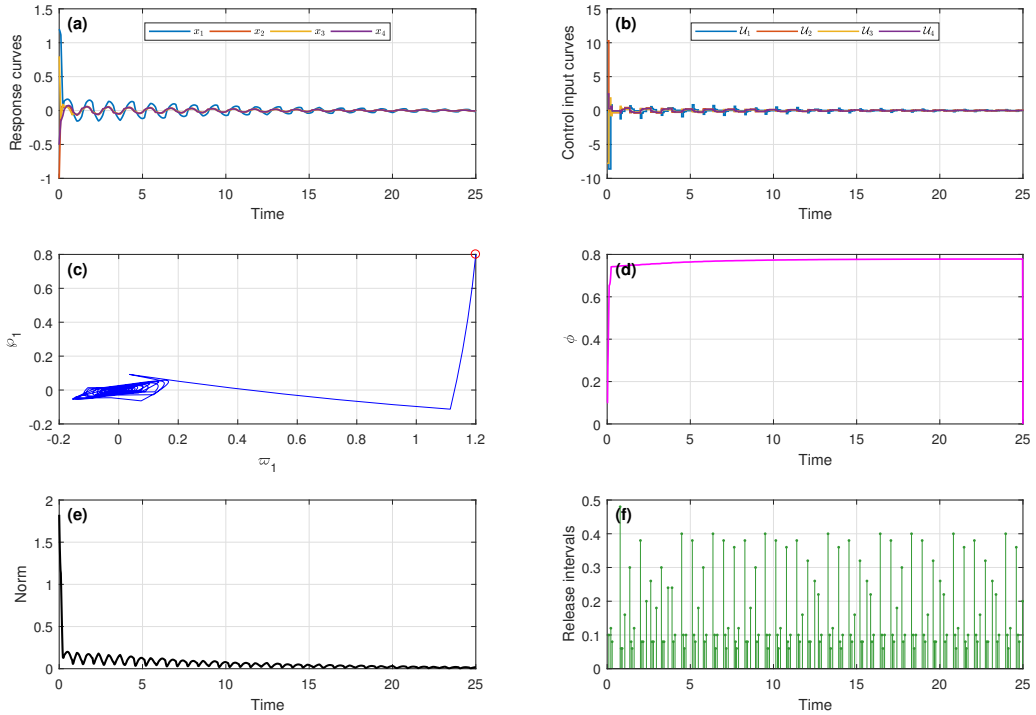

Figure 9. $L_2 - L_\infty$ performance of without attack state responses, control inputs, phase portrait, adaptive threshold response, error norm, and triggered release intervals.

With attack: Figure 10 shows the L_2-L_∞ performance during deception attacks with $\hat{\delta} = 0.2$. In subplot (a), error states converge to zero with slight oscillations. The control inputs in (b) spike briefly but stabilize. Subplot (c) shows asymptotic convergence to the origin from the initial state (red circle). The adaptive evolution of $\phi(t)$ is depicted in (d). Even with short-term increases, the error norm decays in (e). Finally, subplot (f) shows how trigger instants and varying intervals improve communication under attack.

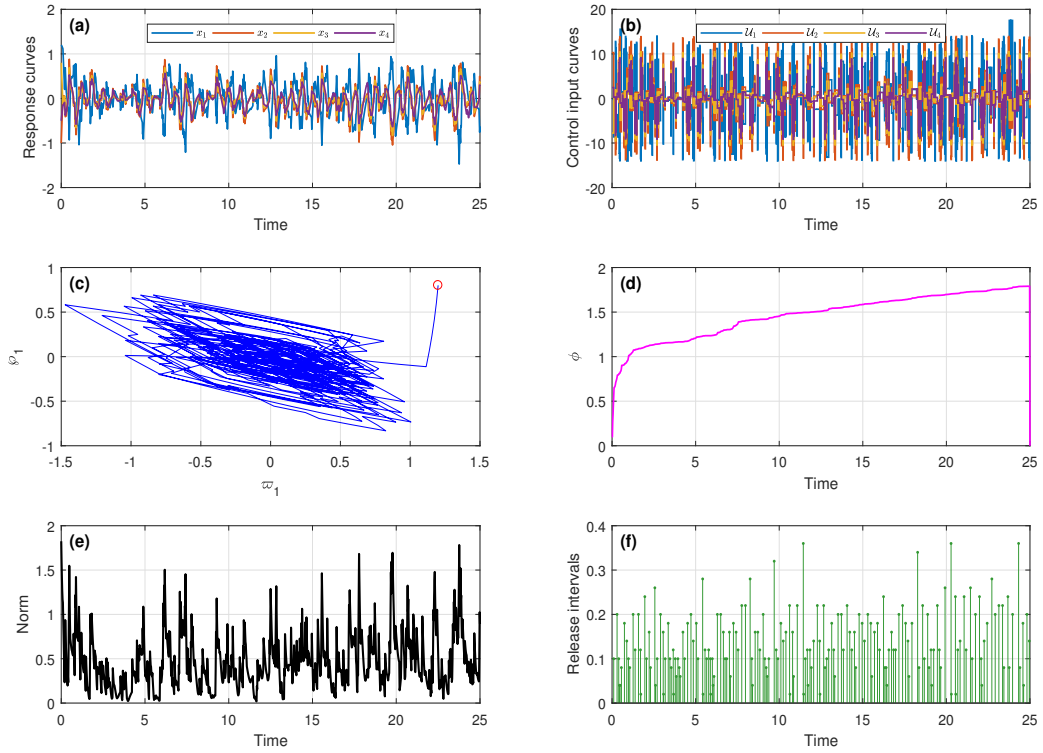

Figure 10. $L_2 - L_\infty$ performance with attack state responses, control inputs, phase portrait, adaptive threshold response, error norm, and triggered release intervals.

Anti-synchronization performance of the INNs in four cases:

Table 3 describes the various labels' meanings in Figures 11–14 subplots. The following Figures 11–14 illustrate the anti-synchronization performance of the INNs across Passivity, (Q, S, R)-dissipativity, H_∞, and $L_2 - L_\infty$ frameworks. The left column represents the system under ideal transmission (No Attack), while the right column depicts the system's robustness under Bernoulli deception attacks. In all plots, the solid blue line represents the master states $(\hat{x}_1, h)$ and the dashed red line represents the slave states $(\hat{x}_2, \hat{h})$.

Table 3. Descriptions of subfigures for Master–Slave anti-synchronization states.

Label	Description
(a)	State response of $\hat{x}_{11}(t)$ vs. $\hat{x}_{21}(t)$ in the absence of attacks.
(b)	State response of $\hat{x}_{11}(t)$ vs. $\hat{x}_{21}(t)$ under Bernoulli deception attacks.
(c)	State response of $\hat{x}_{12}(t)$ vs. $\hat{x}_{22}(t)$ in the absence of attacks.
(d)	State response of $\hat{x}_{12}(t)$ vs. $\hat{x}_{22}(t)$ under Bernoulli deception attacks.
(e)	State response of $h_1(t)$ vs. $\hat{h}_1(t)$ in the absence of attacks.
(f)	State response of $h_1(t)$ vs. $\hat{h}_1(t)$ under Bernoulli deception attacks.
(g)	State response of $h_2(t)$ vs. $\hat{h}_2(t)$ in the absence of attacks.
(h)	State response of $h_2(t)$ vs. $\hat{h}_2(t)$ under Bernoulli deception attacks.

The passivity-based figure plots Figure 11 show a more relaxed anti-synchronization. While the mirroring is achieved successfully in the clean scenario, the system is more susceptible to oscillations under attack due to the lower gain intensity ($atk\_p = 0.25$). The convergence follows a natural energy-decay path, ensuring that the total system energy remains dissipative even if the trajectory appears less stiff than the dissipative or H_∞ cases.

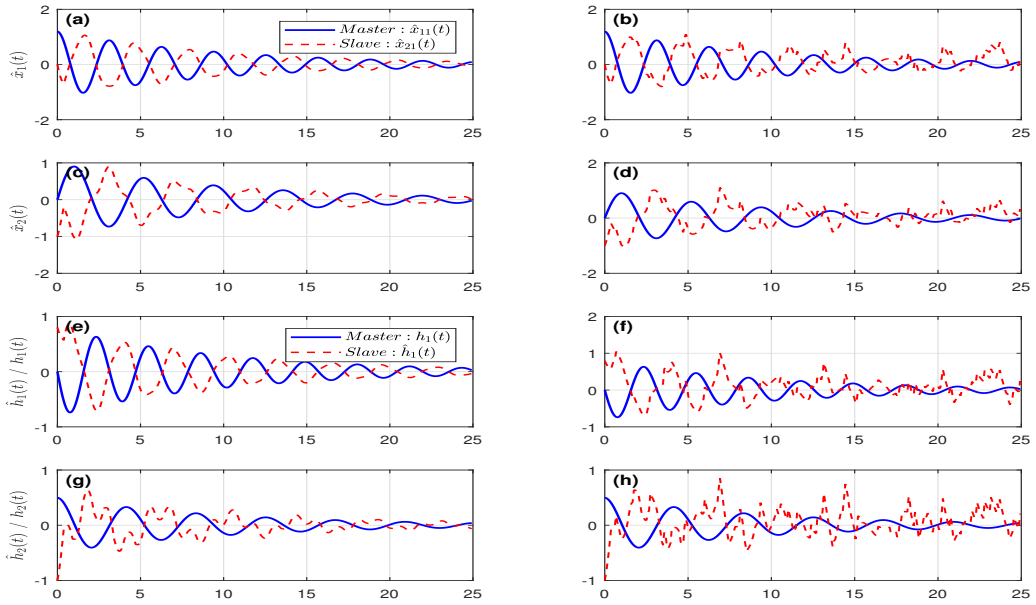

Figure 11. Anti-synchronization trajectories of the INNs under passivity performance with and without deception attacks.

Using a generalized (Q, S, R) framework, this case Figure 12, demonstrates high robust stability with a control gain. The slave system tracks the master with high stiffness. In the attack column, the controller manages a 40% attack probability with minimal chattering. The dissipative criteria ensure that the synchronization error stays within a predefined manifold, balancing the trade-offs between tracking precision and communication resource savings.

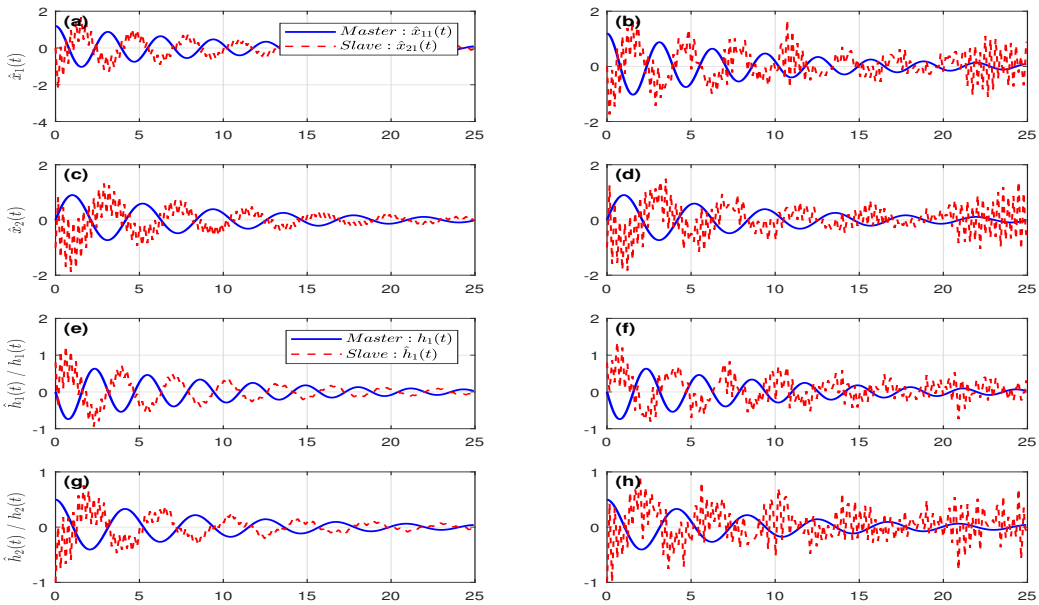

Figure 12. Anti-synchronization trajectories of the INNs under (Q, S, R)- dissipativity performance with and without deception attacks.

This case demonstrates superior disturbance attenuation. Despite a high attack probability (90%), the slave system maintains a tight inverse trajectory to the master, as shown in subplots Figure 13. The H_∞ controller minimizes the L_2-gain of the deception signal, resulting in the most stable mirroring effect among the cases when subjected to high-frequency interference. The chattering in the right column is suppressed effectively, ensuring high-precision synchronization.

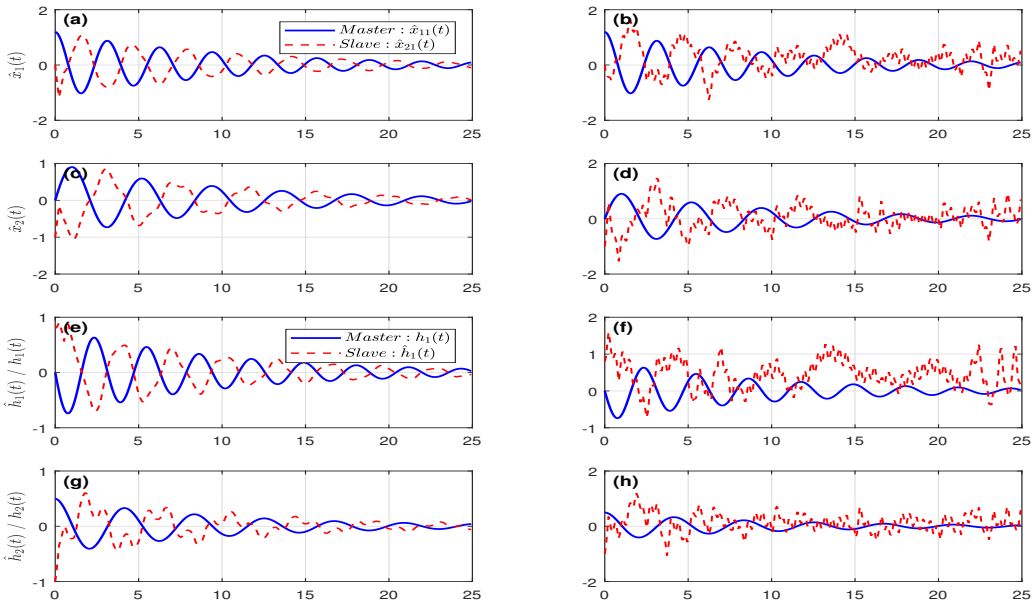

Figure 13. Anti-synchronization trajectories of the INNs under H_∞ performance with and without deception attacks.

The $L_2 - L_\infty$ results prioritize transient peak suppression. In the attack scenario, the dashed red lines exhibit slightly more deviation, but the controller ensures that the peak synchronization error (the maximum distance between the sum of states and the origin) remains strictly bounded in Figure 14.

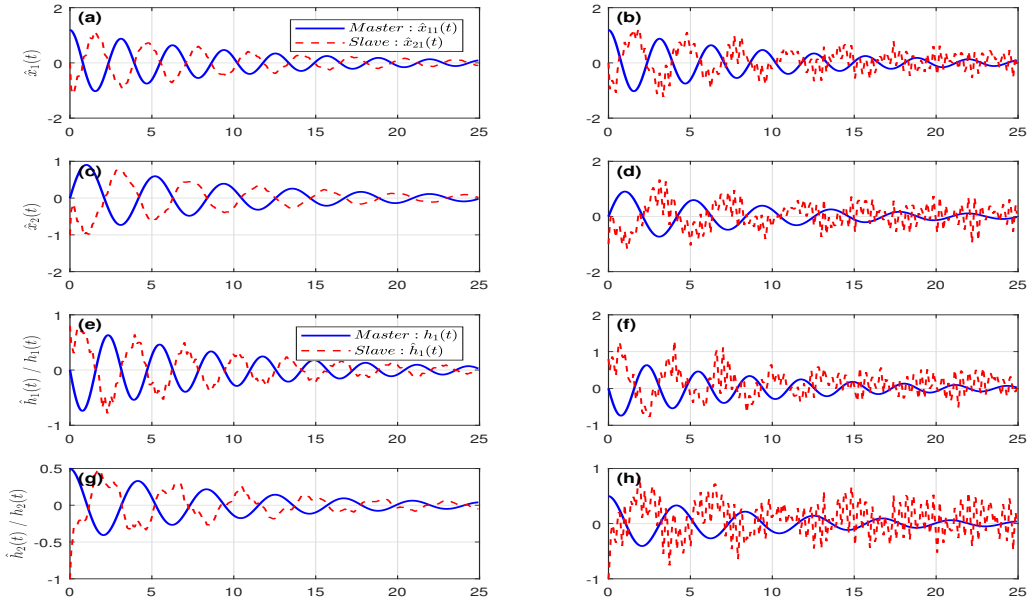

Figure 14. Anti-synchronization trajectories of the INNs under $L_2 - L_\infty$ performance with and without deception attacks.

6. Conclusions

This research has tackled the anti-synchronization issue of INNs with time-varying delays during deception attacks by introducing a dynamic hybrid-triggered control architecture. By integrating extended dissipativity theory with LKF analysis, enough stability requirements were established to ensure robust anti-synchronization performance. The designed control technique efficiently balances communication efficiency and security by dynamically alternating between time-triggered and event-triggered mechanisms. Simulation results validate that the suggested methodology attains enhanced stability, resilience, and minimized communication demands, thereby providing an appropriate and efficient resolution for the secure control of delayed INNs. Future work will concentrate on expanding the suggested framework to encompass more complex network architectures, including stochastic switching topologies, distributed actuator and sensor malfunctions, and multi-agent systems. Furthermore, the integration of adaptive learning mechanisms and empirical validations on actual cyber–physical systems will be examined to improve robustness and practical applicability.

Author Contributions: Conceptualization, P.H.; Methodology, V.R.; Software, V.R.; Writing–original draft, P.H.; Writing–review and editing, V.R.; Supervision, V.R. All authors have read and agreed to the published version of the manuscript.

Funding: This research received no external funding.

Data Availability Statement: No new data were created or analyzed in this study. Data sharing is not applicable to this article.

Conflicts of Interest: The authors declare no conflicts of interest.

Nomenclature

Symbol	Description
$\mathbb{R}^n$	n-dimensional Euclidean space
$\mathbb{R}^{n\times m}$	Set of real matrices of dimension $n \times m$
x^T	Transpose of vector or matrix x
$\|x\|$	Euclidean norm of vector x
I	Identity matrix of appropriate dimension
$\text{diag}\{\cdot\}$	Block diagonal matrix
$Sym\{A\}$	$A + A^T$
$A > 0$ ($A \geq 0$)	Positive definite (positive semi-definite) matrix A
$\lambda_{\min}(A)$, $\lambda_{\max}(A)$	Minimum and Maximum eigenvalue of matrix A
$\mathbb{E}\{\cdot\}$	Expectation operator
$\star$	Symmetric term in matrix inequalities

References

1. Lakshmanan, S.; Prakash, M.; Lim, C.P.; Rakkiyappan, R.; Balasubramaniam, P.; Nahavandi, S. Synchronization of an inertial neural network with time-varying delays and its application to secure communication. *IEEE Trans. Neural Netw. Learn. Syst.* **2016**, *29*, 195–207. [CrossRef] [PubMed]
2. Tu, Z.; Dai, N.; Wang, L.; Yang, X.; Wu, Y.; Li, N.; Cao, J. H_∞ state estimation of quaternion-valued inertial neural networks: Non-reduced order method. *Cogn. Neurodyn.* **2023**, *17*, 537–545.
3. Huang, C.; Liu, B. New studies on dynamic analysis of inertial neural networks involving non-reduced order method. *Neurocomputing* **2019**, *325*, 283–287. [CrossRef]
4. Zhang, B.; Zheng, W.X.; Xu, S. Filtering of Markovian jump delay systems based on a new performance index. *IEEE Trans. Circuits Syst. I Regul. Pap.* **2013**, *60*, 1250–1263. [CrossRef]
5. Wei, H.; Li, R.; Chen, C.; Tu, Z. Extended dissipative analysis for memristive neural networks with two additive time-varying delay components. *Neurocomputing* **2016**, *216*, 429–438. [CrossRef]

6. Seuret, A.; Gouaisbaut, F. Wirtinger-based integral inequality: Application to time-delay systems. *Automatica* **2013**, *49*, 2860–2866. [CrossRef]
7. Park, P.; Ko, J.W.; Jeong, C. Reciprocally convex approach to stability of systems with time-varying delays. *Automatica* **2011**, *47*, 235–238. [CrossRef]
8. Long, F.; Zhang, C.K.; Shen, Y.; Mei, Q.; Chen, Q. Stability analysis of delayed neural networks via novel delay-dependent LKF and integral inequality. *ISA Trans.* **2025**, *165*, 222–231. [CrossRef] [PubMed]
9. Zhang, W.; Li, C.; Huang, T.; Xiao, M. Synchronization of inertial neural networks with time-varying delays via static or dynamic event-based control. *IEEE Trans. Cybern.* **2022**, *52*, 3924–3935.
10. Premalatha, S.; Shanmugapriya, M.; Indumathi, P.; Kumar, S.S. Global dissipative examination of delayed memristive inertial neural networks with uncertain parameters. *Neural Process. Lett.* **2025**, *57*, 83. [CrossRef]
11. Shanmugasundaram, S.; Udhayakumar, K.; Gunasekaran, D.; Rakkiyappan, R. Event-triggered impulsive control design for synchronization of inertial neural networks with time delays. *Neurocomputing* **2022**, *483*, 322–332. [CrossRef]
12. Senan, S.; Ali, M.S.; Vadivel, R.; Arik, S. Decentralized event-triggered synchronization of uncertain Markovian jumping neutral-type neural networks with mixed delays. *Neural Netw.* **2017**, *86*, 32–41. [CrossRef] [PubMed]
13. Wu, A.; Zeng, Z. Anti-synchronization control of a class of memristive recurrent neural networks. *Commun. Nonlinear Sci. Numer. Simul.* **2013**, *18*, 373–385. [CrossRef]
14. Huang, C.; Cao, J. Active control strategy for synchronization and anti-synchronization of a fractional chaotic financial system. *Phys. A Stat. Mech. Its Appl.* **2017**, *473*, 262–275. [CrossRef]
15. Hu, D.; Song, X.; Li, X.; Ma, J. Intermittent control for synchronization of Markov jump inertial neural networks with reaction–diffusion terms via non-reduced-order method. *Circuits Syst. Signal Process.* **2023**, *42*, 199–215.
16. Ali, M.S.; Vadivel, R.; Alsaedi, A.; Ahmad, B. Extended dissipativity and event-triggered synchronization for T–S fuzzy Markovian jumping delayed stochastic neural networks with leakage delays via fault-tolerant control. *Soft Comput.* **2020**, *24*, 3675–3694.
17. Li, M.; Xia, J.; Zhao, J.; Zhang, H.; Shen, H. Event-triggered extended dissipative control for networked singular systems. *Int. J. Control. Autom. Syst.* **2021**, *19*, 382–391. [CrossRef]
18. Shanmugam, S.; Vadivel, R.; Sabarathinam, S.; Hammachukiattikul, P.; Gunasekaran, N. Enhancing synchronization criteria for fractional-order chaotic neural networks via intermittent control: An extended dissipativity approach. *Math. Model. Control* **2025**, *5*, 31. [CrossRef]
19. Wang, J.; Zhang, X.M.; Han, Q.L. Event-triggered generalized dissipativity filtering for neural networks with time-varying delays. *IEEE Trans. Neural Netw. Learn. Syst.* **2015**, *27*, 77–88.
20. Albea, C.; Seuret, A. Time-triggered and event-triggered control of switched affine systems via a hybrid dynamical approach. *Nonlinear Anal. Hybrid Syst.* **2021**, *41*, 101039. [CrossRef]
21. Leen, G.; Heffernan, D. TTCAN: A new time-triggered controller area network. *Microprocess. Microsyst.* **2002**, *26*, 77–94. [CrossRef]
22. Varma, V.S.; de Oliveira, A.M.; Postoyan, R.; Morărescu, I.C.; Daafouz, J. Energy-efficient time-triggered communication policies for wireless networked control systems. *IEEE Trans. Autom. Control* **2019**, *65*, 4324–4331.
23. Heemels, W.P.; Johansson, K.H.; Tabuada, P. An introduction to event-triggered and self-triggered control. In *Proceedings of the 2012 IEEE 51st IEEE Conference on Decision and Control (CDC)*; IEEE: Piscataway, NJ, USA, 2012; pp. 3270–3285.
24. Vadivel, R.; Joo, Y.H. Robust event-triggered T–S fuzzy system with successive time-delay signals and its application. *IET Control Theory Appl.* **2020**, *14*, 3697–3712. [CrossRef]
25. Vadivel, R.; Sabarathinam, S.; Zhai, G.; Gunasekaran, N. Event-triggered reachable set estimation for synchronization of Markovian jump complex-valued delayed neural networks under cyber-attacks. *Eur. Phys. J. Spec. Top.* **2025**, *234*, 3683–3703.
26. Vadivel, R.; Hammachukiattikul, P.; Zhu, Q.; Gunasekaran, N. Event-triggered synchronization for stochastic delayed neural networks: Passivity and passification case. *Asian J. Control* **2023**, *25*, 2681–2698. [CrossRef]
27. Li, F.; Hou, Z. Event-triggered model-free adaptive predictive control for networked control systems under deception attacks. *IEEE Trans. Syst. Man Cybern. Syst.* **2023**, *54*, 1325–1334.
28. Wang, X.; Park, J.H.; Li, H. Fuzzy secure event-triggered control for networked nonlinear systems under DoS and deception attacks. *IEEE Trans. Syst. Man Cybern. Syst.* **2023**, *53*, 4165–4175. [CrossRef]
29. Kazemy, A.; Lam, J.; Zhang, X.M. Event-triggered output feedback synchronization of master–slave neural networks under deception attacks. *IEEE Trans. Neural Netw. Learn. Syst.* **2020**, *33*, 952–961.
30. Liu, X.M.; Chang, X.H.; Hou, L.W. Attack-dependent adaptive event-triggered security fuzzy control for nonlinear networked cascade control systems under deception attacks. *Mathematics* **2024**, *12*, 3385. [CrossRef]
31. Dou, Z.; Ding, L.; Yan, S. Dynamic integral-event-triggered control of photovoltaic microgrids with multimodal deception attacks. *Symmetry* **2025**, *17*, 838. [CrossRef]